

REPORT DOCUMENTATION PAGE

1a. REPORT SECURITY CLASSIFICATION Unclassified		1b. RESTRICTIVE MARKINGS	
2a. SECURITY CLASSIFICATION AUTHORITY AD-A209 018		3. DISTRIBUTION / AVAILABILITY OF REPORT Approved for public release; distribution unlimited.	
6a. NAME OF PERFORMING ORGANIZATION Massachusetts Institute of Technology, Civil Engineering		5. MONITORING ORGANIZATION REPORT NUMBER(S) ARO 24620-15-EG-UIR	
6b. ADDRESS (City, State, and ZIP Code) 77 Massachusetts Avenue, Room 1-175 Cambridge, MA 02139		7a. NAME OF MONITORING ORGANIZATION U. S. Army Research Office	
6c. ADDRESS (City, State, and ZIP Code) P. O. Box 12211 Research Triangle Park, NC 27709-2211		7b. ADDRESS (City, State, and ZIP Code) P. O. Box 12211 Research Triangle Park, NC 27709-2211	
8a. NAME OF FUNDING / SPONSORING ORGANIZATION U. S. Army Research Office		8b. OFFICE SYMBOL (If applicable) CCRE/PACT	
9. PROCUREMENT INSTRUMENT IDENTIFICATION NUMBER DAAL03-87-K-0005		10. SOURCE OF FUNDING NUMBERS	
		PROGRAM ELEMENT NO.	PROJECT NO.
		TASK NO.	WORK UNIT ACCESSION NO.
11. TITLE (Include Security Classification) Mechanics of Damage in Rate-Sensitive Construction Materials			
12. PERSONAL AUTHOR(S) Shyam Sunder, W.; Wu, Maos			
13a. TYPE OF REPORT Technical		13b. TIME COVERED FROM 1/87 TO 12/87	
14. DATE OF REPORT (Year, Month, Day) December 30, 1987		15. PAGE COUNT 119	
16. SUPPLEMENTARY NOTATION The view, opinions and/or findings contained in this report are those of the author(s) and should not be construed as an official Department of the Army position			
17. COSATI CODES		18. SUBJECT TERMS (Continue on reverse if necessary and identify by block number)	
FIELD	GROUP	SUB-GROUP	
		Damage mechanics; rate-sensitive construction materials; Damage models; advanced construction materials	
19. ABSTRACT (Continue on reverse if necessary and identify by block number) The objective of this research is to develop an understanding of and characterize the rate and damage processes and their interaction in advanced construction materials. This report presents: a multiaxial differential flow model; a rate and pressure sensitive anisotropic damage model; and, specification for testing materials.			
20. DISTRIBUTION / AVAILABILITY OF ABSTRACT <input type="checkbox"/> UNCLASSIFIED/UNLIMITED <input type="checkbox"/> SAME AS RPT. <input type="checkbox"/> DTIC USERS		21. ABSTRACT SECURITY CLASSIFICATION Unclassified	
22a. NAME OF RESPONSIBLE INDIVIDUAL		22b. TELEPHONE (Include Area Code)	22c. OFFICE SYMBOL

MECHANICS OF DAMAGE
IN RATE-SENSITIVE CONSTRUCTION MATERIALS

TECHNICAL REPORT

By

Professor S. Shyam Sunder
Associate Professor of Civil Engineering

Mao S. Wu
Graduate Research Assistant


DECEMBER 30, 1987

U.S. ARMY RESEARCH OFFICE
Contract No. DAAL03-87-K-0005

MASSACHUSETTS INSTITUTE OF TECHNOLOGY

APPROVED FOR PUBLIC RELEASE;
DISTRIBUTION UNLIMITED

Accession For	
NTIS GRA&I	<input checked="checked" type="checkbox"/>
DTIC TAB	<input type="checkbox"/>
Unannounced	<input type="checkbox"/>
Justification	
By	
Distribution/	
Availability Codes	
Dist	Avail and/or Special
A-1	



THE VIEWS, OPINIONS, AND/OR FINDINGS CONTAINED IN THIS REPORT ARE THOSE OF THE AUTHORS AND SHOULD NOT BE CONSTRUED AS AN OFFICIAL DEPARTMENT OF THE ARMY POSITION, POLICY, OR DECISION, UNLESS SO DESIGNATED BY OTHER DOCUMENTATION.

Accession For	
NTIS GRA&I	<input checked="checked" type="checkbox"/>
DTIC TAB	<input type="checkbox"/>
Unannounced	<input type="checkbox"/>
Justification	
By	
Distribution/	
Availability Codes	
Dist	Avail and/or Special
A-1	

1. TABLE OF CONTENTS

	<u>Page</u>
1. TABLE OF CONTENTS.....	1
2. LIST OF APPENDICES.....	2
3. TECHNICAL REPORT.....	3
A. Statement of Problem.....	3
Introduction.....	3
Objectives of Research.....	4
B. Summary of Research Accomplishments.....	4
Multiaxial Differential Flow Model.....	5
Rate-Sensitive Continuum Damage Model.....	11
Experimental Facilities and Program.....	17
C. List of Publications.....	19
D. List of Participating Scientific Personnel.....	19
4. BIBLIOGRAPHY.....	20
5. APPENDICES.....	22
Appendix A	
Appendix B	

2. LIST OF APPENDICES

- Appendix A - A MULTIAXIAL DIFFERENTIAL FLOW LAW FOR
POLYCRYSTALLINE ICE (49p.)
- Appendix B - A RATE-SENSITIVE CONTINUUM DAMAGE MODEL FOR ICE
(45p.) - Draft Manuscript

3. TECHNICAL REPORT

A. STATEMENT OF PROBLEM

Introduction: Rate mechanisms govern the mechanical behavior of construction materials under three conditions: (1) at high homologous temperatures; (2) when subjected to short term loading that is quasi-static, impulsive, or vibratory; and (3) when subjected to sustained (or creep) loading over long times. Examples of advanced construction materials satisfying one or more of these conditions include:

- (a) Polymer matrix structural composites such as FRPs;
- (b) Single-ply roofing membranes made of elastomers;
- (c) Polycrystalline ice in cold regions engineering;
- (d) Cementitious composites such as high-strength concretes and FRCs.

The deformation and progressive failure of such rate sensitive materials is governed by three primary mechanisms: flow, distributed cracking, and localized crack propagation. The interaction of these mechanisms gives rise to complex mechanical behavior on the macro-scale. The characterization of these mechanisms and their interaction is therefore of fundamental importance. → see #142

Any given material may display purely ductile, purely brittle or combined behavior depending upon the temperature and conditions of loading. The primary mechanism of flow and the constitutive framework of rate process theory are appropriate for characterizing purely ductile behavior. The primary mechanism associated with distributed cracking and the constitutive framework of damage theory are appropriate for characterizing deformations during ductile-to-brittle transition or when the material is purely brittle. Such deformations are accompanied by the formation and stable growth of cracks and/or voids. The primary mechanism associated with localized cracking and fracture mechanics theory are appropriate for predicting the onset of material instability.

Damage processes control failure in engineering materials

prior to localization of fracture (formation and propagation of a single crack). Consequently, the ultimate strength of such materials is generally governed by damage. In addition, damage plays an important role in defining the onset of material instability during localized fracture. The phenomenon of damage is particularly significant when the state of stress involves compression.

Objectives of Research: The objective of this research is to understand and characterize rate and damage processes and their interaction in advanced construction materials. Both theoretical and experimental research are being pursued. In particular, the following three tasks are being undertaken:

(a) The modeling of both transient and steady state flow in orthotropic materials based on physical processes occurring on the micro-scale.

(b) The development of an anisotropic damage model which takes into account the damage processes leading to progressive deterioration of material integrity. Specifically, the rate and pressure sensitivity of the damage processes are investigated.

(c) The development of an experimental capability for testing materials at low temperatures, under high rates of loading, and under high confining pressures. The program of experimentation is being designed to verify the theoretical models of flow and damage.

Three classes of materials are under consideration: homogeneous and isotropic; homogeneous but anisotropic; non-homogeneous, but isotropic (e.g., random short-fiber reinforced composites).

B. SUMMARY OF RESEARCH ACCOMPLISHMENTS

Research during the past year has led to the development of (i) a multiaxial differential flow model, (ii) a rate and pressure sensitive anisotropic damage model, and (iii) specifications for testing materials as described Section 4.A. The technical approach and the most important results are summarized here. The details are contained in Appendices A and B

which are technical papers written for the flow and damage models, respectively, with specific applications to polycrystalline ice. This material has been chosen for the initial phase of this research since it displays a wide spectrum of behaviors typical of many other materials. The dominant behavioral mode is strongly dependent on the rate and history of loading, as well as the ambient temperature. Furthermore, isotropic polycrystalline ice is an ideal testing material for verifying the damage model due to its (i) transparency which facilitates visual correlation of cracking activity with quantitative acoustic emission studies, and (ii) homogeneity and isotropy which lend itself easily to the basic verification of theoretical aspects such as damage induced anisotropy predicted by the evolution laws of the model.

MULTIAXIAL DIFFERENTIAL FLOW MODEL

Physical Basis.-- Flow (or creep) is modeled in terms of the physical mechanisms operating on the micro-scale. In polycrystalline ice, it is known from both theoretical and experimental work that at least two deformation systems, a soft system and a hard system, are present during flow. These include grain boundary sliding and basal slip, or basal slip and slip on a non-basal plane.

Under load the material initially resists the applied stress in an elastic manner and then flow begins on the soft and hard systems. Flow, particularly on the easy soft system, causes the build up of internal elastic stresses. This may occur as a result of grain boundary sliding next to grains poorly aligned for deformation or dislocation pile-ups at the boundaries of such grains. These internal elastic stresses are known as the back or rest stresses. In addition, internal drag stresses which resist dislocation fluxes and sliding are generated by (a) creep resistant substructures, i.e. subgrains and cells, formed by grain boundary sliding or dislocation movement, and (b) dislocation entanglement, dipole formation, and kink band formation during slip.

An increasing back stress contributes to kinematic hardening which induces directionally dependent material behavior, referred to as deformation induced anisotropy. The Baushinger effect in metals is an example of kinematic hardening. On the other hand, an increasing drag stress contributes to isotropic hardening. In isotropic hardening, subsequent material properties are independent of the direction of pre-straining.

In the model the total deformation resulting from the interaction between the soft and hard systems is decomposed into a transient component and a steady state component. Isotropic and kinematic hardening phenomena are active during transient flow and give rise to elastic strains which are recoverable upon unloading. These time-dependent elastic strains represent delayed elasticity or anelasticity. Steady state flow is associated with viscous strains which are irrecoverable. Such viscous deformation is attributed to intragranular deformation processes, especially to the movement of dislocations. When transient flow has become saturated, hardening effectively ceases and pure viscous flow results.

Mathematical Formulation.-- All equations stated in connection with the Multiaxial Differential Flow Model refer to those in Appendix A. The uniaxial governing equation is obtained by expressing the total strain rate as a sum of the transient and steady state flow components, as well as the elastic component associated with instantaneous deformation (Eq. (1)). The instantaneous component is described by the classical theory of linear elasticity which in rate form relates the elastic strain rate to the stress rate through the Young's modulus (Eq. (2)). The viscous strain follows the well-known power law of Glen (1955), i.e. the viscous strain rate is proportional to the third power of stress (Eq. (3)). The constant in Glen's law is temperature dependent and follows the Arrhenius activation energy law (Eq. (4)). The transient strain rate is also taken to follow Glen's law with the same temperature dependence, but transient flow is now driven by a reduced stress quantity, equal to the ratio of the applied stress less the back stress to a

dimensionless drag stress (Eq. (5)).

Since the back and drag stresses are history dependent variables associated with transient flow, evolution equations must be specified for them. Due to the elastic nature of the recoverable transient strains, the time rates of change of the back and drag stresses can be assumed to be proportional to the transient strain rate itself. These evolution equations are stated in Eqs. (6) and (7).

Under creep loading Eq. (6) predicts that the back stress will asymptotically increase to a value equal to the applied stress, at which point transient flow will cease. Under constant strain rate loading the back stress will asymptotically attain the value of the steady-state stress. For either loading condition, the drag stress will also reach its limiting value when transient flow ceases. Under reversed or cyclic loading the back stress will reverse or switch back between positive and negative values, i.e., the physical processes associated with kinematic hardening can locally relax or move back and forth between positive and negative values. During reversed loading, the drag stress will also decrease, indicating a decreasing resistance to transient flow. On the other hand, the drag stress will reach a saturated value under cyclic loading, while the back stress will eventually switch back and forth between some limiting values.

Model Formulation in Dimensionless Variables.-- Based on the test data of Jacka (1984) for isotropic polycrystalline ice, Ashby and Duval (1985) have suggested that unique relationships exist between certain dimensionless variables. Such relationships are predicted by the proposed model as explained below.

Under constant stress loading the model predicts that the relationships between dimensionless strain, strain rate and time are independent of the applied stress and temperature. The dimensionalization is achieved by expressing the dimensionless variables as ratios between the variables and their appropriate normalizing variables, i.e., all strain quantities are normalized with the elastic strain, all strain rate quantities with the

steady viscous strain rate, and all stress quantities with the applied stress (Eqs. (8), (9), (11)). Dimensionless time is defined as time multiplied by the viscous strain rate divided by the elastic strain (Eq. (10)). It is possible to express the equations of the model as well as the evolution equations in terms of these dimensionless variables (Eqs. (12)-(17)), thus predicting unique relationships (i.e., independent of the applied stress and temperature) between them.

In the case of constant strain rate loading, the model predicts that a unique relationship exists between the dimensionless stress and time (or strain). The dimensionalization is achieved by normalizing all strain variables with the elastic strain, and all stress variables with the steady-state stress (Eqs. (18), (20)). The steady-state stress is given by Glen's power law for viscous flow, Eq. (21). Dimensionless time is defined as time multiplied by the constant strain rate divided by the maximum elastic strain (Eq. (19)). The equations of the model and the governing equations can be expressed in terms of these dimensionless variables (Eqs. (22)-(27)). Since the temperature dependent constant associated with Glen's law and the applied constant strain rate have been eliminated from these equations, a unique master curve can be used to relate the dimensionless stress and time.

Experimental Validation of Uniaxial Model.-- The uniaxial model is verified against the constant stress (creep) data of Jacka (1984) and Sinha (1978). The former data set is obtained from tests conducted on isotropic polycrystalline ice with an average grain size of 1.7 mm, whereas the latter is obtained from tests conducted on columnar-grained ice with an average grain size of 3 mm. To further demonstrate the capability of the model, the predicted strain response under a monotonically increasing stress is verified against Sinha's (1981) data for columnar-grained ice with an average grain size of 4.5 mm. Finally, the creep and recovery response of randomly oriented snow ice is studied using Brill and Camp's data taken from Sinha (1979). Note that all figures mentioned in this subsection refer

to those in Appendix A.

Figures 1-3 show Jacka's data together with the model predictions (curves (b)) using dimensionless variables. As can be seen from these figures, unique relationships between dimensionless strain rate and time, between dimensionless strain rate and strain, and between dimensionless strain and time, are fully justified by the test data corresponding to various stress levels and temperatures.

Excellent agreement between model prediction and Sinha's creep data for various temperatures is demonstrated in Fig. 4. Under a monotonically increasing stress history, the predicted strain-time and stress-strain relationships also agree well with Sinha's test data, as shown in Fig. 6.

Figure 7 shows three sets of creep and recovery data obtained under different conditions of stress and temperature. The model predictions for both creep and recovery agree fairly well with the data.

Multiaxial Model Formulation.-- The three-dimensional generalization of the uniaxial model follows from the uniaxial formulation, i.e., it is based on strain decomposition, linear elasticity, and the rate theory of flow. Constitutive relations are derived for each mechanism of deformation in the model, resulting in the orthotropic equivalent of Eqs. (1)-(7).

Orthotropic elasticity (Eq. (44)) follows the classical theory (see, for example, the book by Lekhnitskii, 1963). The orthotropic generalization of viscous flow is derived from the normality of the viscous strain rate to a scalar-valued viscous flow potential defined in terms of an equivalent stress measure (see Eqs. (45)-(52)). The equivalent stress measure with six orthotropic constants is a generalized form for orthotropic materials. An equivalent strain or strain rate measure (Eq. (56)) for orthotropic materials can also be derived based on the hypothesis of energy equivalence. The orthotropic generalization of transient flow is based on the assumption of flow incompressibility. Furthermore, the material orthotropy is described by the same set of orthotropic constants mentioned

previously. In a manner similar to the derivation of the viscous strain rate, the equation for transient flow is derived from the normality of the transient strain rate to a scalar-valued transient flow potential defined in terms of an equivalent reduced stress measure. Note that since incompressibility of flow is assumed, all stress and strain quantities used in the equations for viscous and transient deformations are deviatoric. The resulting expression is expressed in Eq. (58). Evolution equations are also generalized to three dimensions where the appropriate variables are the deviatoric back stress vector and a scalar equivalent drag stress (Eqs. (63) and (64)). The constraint condition (i.e., strain decomposition), the equations for orthotropic elasticity, viscous and transient strain rates, together with the evolution equations form the equations of the multi-axial model which can be numerically integrated to predict the model response under variable loading histories.

Experimental Validation of Multi-axial Model.-- In this subsection the x-axis is taken to be normal to the columnar ice sheet which is defined by the y-z plane. The columns of the ice sheet are parallel to the growth direction, i.e. along the x-axis. The c-axes of the ice crystals are assumed to lie in the y-z plane and are aligned in the y-direction.

The model response is verified against Frederking's (1977) data obtained from plane strain compression tests on columnar-grained transversely isotropic (a special case of orthotropy in which parallel planes of isotropy exist in the material) freshwater ice. The planes of isotropy are the y-z planes. The orthotropic constants can be determined from uniaxial tests (see Eq. (69) for details). In his type A tests, strains in the z-direction are constrained to zero and stresses are applied in the y-direction. At steady state where the power law orthotropic formulation suffices, the ratio of the plane strain stress to the unconfined stress at the same strain rate (Eq. 74) is predicted to vary between 2.1-5.1. These values are consistent with Frederking's experimental observations which were close to 2 at high strain rates and to 5 at low strain rates. In his type B

tests, strains in the x-direction are constrained to zero while stresses are again applied in the y-direction. The predicted ratio between the plane strain stress and the unconfined stress at the same strain rate (Eq. 75) varies between 1.01 and 1.06, which again agrees with Frederking's test results which showed negligible influence of x-direction confinement on stresses.

RATE-SENSITIVE CONTINUUM DAMAGE MODEL

Rationale For the Use of Damage Variable in Constitutive Modeling.-- The theory of plasticity, originally developed as a phenomenological theory for modeling nonlinear material behavior due to such irreversible processes as crystalline slip and twinning, is generally found to be unsuitable for the description of material behavior dominated by the nucleation and growth of microcracks. Conventional fracture mechanics, on the other hand, is concerned with the prediction of material response dominated by a single macrocrack. However, there are many instances when the material deteriorates by the nucleation and stable growth of a multitude of stable microcracks (damage) distributed over the entire material continuum, especially when the material is loaded in compression. Depending on the rate of loading and the stress state, the evolution of damage may significantly affect material behavior and the flow model by itself is therefore insufficient for a proper description of material behavior.

The prediction of the development of damage under different strain rates and stress states is thus of considerable importance if an accurate prediction of material behavior is to be obtained. Since it is desired to study the development of damage per se, isotropic polycrystalline ice is chosen as a material for study where the complexity of material anisotropy is absent. Furthermore, ice also displays rate and pressure sensitive behavior.

During the creep damage process, the nucleation and growth of microcracks can be influenced by diffusion, by dislocation creep, and by stress concentrations at irregularities on grain boundaries caused by grain boundary sliding (Sinha, 1984). These

processes are linked to the development of creep strain, which therefore affects damage growth. On the other hand, damage can be suppressed by a confining pressure. Under low strain rate loading, microcracking is insignificant and the application of a hydrostatic state of confining stress does not increase the maximum shear stress that can be sustained by the material. Under high strain rate loading, damage is significant and application of pressure suppresses the damage, as a result of which a higher shear strength can be sustained by the material. The ratio of the confined shear strength to the unconfined shear strength in the case when there is considerable damage suppression is greater than that in the case when almost pure flow with little damage dominates the material response. This phenomenon is known as pressure sensitivity. Under very large confining pressures the material may undergo pressure melting, and its ability to sustain shear decreases and eventually vanishes at the pressure corresponding to phase change.

Damage in ice leads to "strain softening" under constant strain rate loading, and to accelerating or tertiary creep under constant stress loading. Since a reduction in elastic modulus is observed during unloading (Jordaan, 1986), it can be inferred that damage affects the elastic (in addition to creep) properties of ice as well. Furthermore, the microcracks that have been observed in ice can be approximated as planar in shape, and they are oriented with their normals in the positive principal stress directions (Sinha, 1982). Such induced anisotropy is also observed in many materials and is especially important under non-proportional loading when conditions for rupture or failure depends on the particular loading history of the material, and hence the orientation of the microcracks (Chaboche, 1982, Murakami and Ohno, 1981). Consequently, in modeling damage a scalar representation is inadequate and a vectorial or tensorial approach is necessary.

The model presented here is based on the assumption of an initially isotropic material and takes into account strain rate and pressure sensitivity, pressure melting and damage-induced

anistropy. It uses a second order damage tensor representation introduced by Murakami and Ohno (1981). Damage effects are incorporated through the use of a net stress tensor. This is based on the concept of locally magnified stresses arising from a reduction in load bearing area due to damage. The evolution equations consider damage induced by both local tensile and shear stresses. The damage model is incorporated in the flow model through the use of an averaged net stress tensor, i.e., the stress tensor in the flow model is replaced by the averaged net stress tensor.

Continuum Damage Modeling.-- To predict material response when damage effects are not negligible, it is necessary to (i) select an appropriate damage variable based on some averaging over a representative volume, (ii) establish the damage evolution laws, and (iii) formulate an appropriate set of constitutive relations which incorporate the effects of damage. Note that all equations below refer to those in Appendix B.

The microcracks are directly used to define the damage tensor through the reduction in the strength of sections. This is therefore a geometric approach. For an elementary volume of the damaged material continuum associated with a material point, it has been shown that the damage state can be defined by a second order symmetric tensor (Eq. (1)). This damage tensor is constructed by taking the tensor product of the k^{th} unit vector normal to the k^{th} planar microcrack with itself, integrating over the area of the microcrack, and summed for all microcracks in the elementary volume. Since the resulting tensor is second order symmetric, it can be written in terms of its three principal values and principal directions (Eq. (2)), i.e., as a sum of the three tensor products between the unit vectors representing the principal directions with themselves, where each tensor product is multiplied by the corresponding principal value. This implies that an arbitrary damage field can be described in terms of three mutually orthogonal systems of parallel microcracks. The effect of a multitude of damage fields is in general obtained by summing the different damage tensors (one for each field).

A net stress tensor can be used to represent the locally magnified stress which governs the evolution of damage. Mathematically it can be defined as the symmetric part of the Cauchy stress multiplied by a damage effect tensor (see Eq.(8)). The damage effect tensor is equal to the inverse of the difference between the identity tensor and the damage tensor (see Eq. (9).) Physically the damage effect tensor can be thought of as a quantity representing the effect of local stress concentration which influences damage growth. Since at the present the emphasis is on the study of how damage evolves and not how damage affects the three dimensional deformation behaviour, an averaged net stress is used to specify the constitutive relations. This averaged tensor is defined as the mean of the diagonal components of the damage effect tensor multiplied by the stress tensor (Eq. (10)).

Evolution Equations of Damage.-- The net stress tensor is used to specify the evolution laws. To avoid cumbersome terminology, it is understood that in this subsection all stresses refer to net stresses. It has been experimentally observed for many materials that microcracks tend to form in planes perpendicular to the local principal tensile stresses (Murakami and Ohno, 1981; Costin, 1983). Under a non-hydrostatic compressive state of stress (which is the stress state considered here), local tensile stresses can arise from material property mismatch between grains or from contact stresses between grains with irregular grain boundaries (Costin, 1983). Since the normals to the microcracks formed under compression are usually oriented in the directions of the principal tensile deviatoric stresses, it can be assumed that the local tensile stresses act in the same directions. In the proposed model it is further assumed that such microcracks form only in the planes perpendicular to the maximum local principal tensile deviatoric stress. The "directionality" of anisotropic damage associated with microcracks formed under local tension can then be determined by the tensor product of the unit vector in the direction of the maximum local principal tensile deviatoric stress with itself.

The spherical or hydrostatic state of stress is known to suppress the formation and growth of microcracks. This phenomenon is also observed in ice (Mellor, 1983), especially at high rates of loading. In the evolution laws this effect is modeled by reducing the damage due to the maximum local stress by an amount proportional to the hydrostatic stress.

In addition to the maximum local tensile stress, local shear stresses may also generate microcracks. Such local stresses may be regarded as related to the second invariant of the deviatoric stress tensor, and the microcracks generated in this manner give rise to off-diagonal components in the damage tensor. However, the damage tensor can be transformed to give principal normal values on the main diagonal only. The directionality associated with the second invariant of the stress deviator may be approximately regarded as isotropic since the majority of the shear cracks tend to be randomly orientated with respect to the global frame and will consequently give rise to equal components in all three principal directions. Thus, local shear stresses are assumed to contribute to "isotropic" damage.

To take into account the effect of strain rate on damage, it is proposed that a power law holds between damage growth rate and the effective total strain rate (Murakami et al., 1986). Furthermore, the effects of local stress concentration on damage evolution are modeled by using a scalar invariant of the damage effect tensor for the isotropic part of the damage evolution laws, and by using the magnitude of the damage effect in the direction of the maximum principal stress deviator for the anisotropic part. The complete evolution equations are given by Eqs. (13)-(15).

Constitutive Relations.-- The constitutive laws used here are based on a simple nonlinear generalization of the Maxwell model. Details are given in Appendix B, where the constitutive relations are given by Eqs. (19)-(22). The flow model described earlier is in the process of being implemented and will supercede the Maxwell model. The essential concept in incorporating damage effects in the constitutive relations, however, is to replace the

stress components by appropriate net stress components. As described earlier, averaged net stress components are used, implying that the average damage effect on the global stress is isotropic. This is only true when damage effect is small (Murakami and Imaizumi, 1982). Research is being undertaken to use a better representation of the form of the net stress for use in the constitutive relations.

Pressure Melting Model.-- Ice is known to change phase at a certain level of hydrostatic stress. Triaxial testing of ice was carried out relatively recently (see, for example, Jones, 1982). It is experimentally observed that the resistance of ice to shear stress decreases when hydrostatic stress reaches some moderate level. Thus the flow resistance parameter in Glen's power law should decrease with increase in hydrostatic stress. On the other hand, it is also known that this parameter will decrease with increase in temperature according to the Arrhenius law. Thus, its variation with pressure can be modeled through a temperature correction using the phase diagram for ice. The phase diagram plots the pressure-temperature relationship corresponding to phase change. The relation between the flow parameter and the corrected temperature is then obtained using the Arrhenius law.

Experimental Validation.-- The damage model is verified against several independent sets of data, including the uniaxial data of Gold reproduced in Mellor (1983), and the triaxial data of Jones (1982). The maximum stress is plotted against the strain rate in Fig. 7, which shows Gold's data for various ice types tested under uniaxial compression at -10°C , as well as the model prediction. The agreement between theory and data is excellent. These results show that damage is insignificant at strain rates below about 10^{-4} s^{-1} where deformation is dominated by pure flow. Thus the maximum stress or strength of the material increases with strain rate according to Glen's power law. For strain rates greater than 10^{-4} s^{-1} , i.e., in the ductile-to-brittle transition region, damage becomes significant and the strength becomes less than that predicted by the power law, but still increases monotonically until a plateau is reached at very high strain

rates.

The data of Jones for isotropic polycrystalline ice is obtained from triaxial tests conducted at -12°C . The confining pressure and the strain rate of compressive loading are varied in order to study their effects on the shear strength. The data and the model predictions agree well, thus validating the damage model with regard to the effects of strain rate, stress state and pressure melting. Specifically, these results show that (i) shear strength increases with the applied constant strain rate, (ii) shear strength increases with moderate confining pressure, and (iii) pressure melting lowers the shear resistance. Furthermore, the damage theory predicts that damage is predominantly anisotropic (i.e., microcracks are preferentially oriented perpendicular to the maximum principal stress deviator) when there is no confinement, but a moderate level of confining stress causes the formation of shear microcracks, giving isotropic damage. Anisotropic damage becomes relatively less significant with increase in confining pressure. Ultimately at very high pressure, damage growth is almost entirely associated with the second invariant of the stress deviator, and the material undergoes pseudo-flow with many distributed microcracks.

EXPERIMENTAL FACILITIES AND PROGRAM

The experimental facilities include a low temperature materials testing facility, a load frame and a triaxial cell required for mechanical testing, acoustic emission monitoring system with host computer, transducers and multi-channel monitoring system, and a data acquisition system composed of a microprocessor/controller and a high speed analog to digital converter. Part of the equipment has been purchased and installed with partial ARO support during 1987. Additional funding has been requested from ARO for the remaining equipment needs (load frame, triaxial cell, acoustic emission monitoring system.)

Low Temperature Materials Testing Facility.-- This consists of three cold rooms, a test chamber, a growth room and a storage room. The minimum temperature in the test chamber can reach -40°C

and the precision of the temperature can be controlled to within $\pm 1^{\circ}\text{C}$. The growth room is used for growing ice samples by freezing distilled, degassed and deionized water at 0°C through seed ice crystals. The temperature range in this room lies between -10 and 0°C and the temperature precision is within $\pm 1^{\circ}\text{C}$. The storage room is used for storing ice samples and seed crystals, and as a buffer between the other two rooms and the exterior. Its temperature range is the same as that for the growth room, but the temperature precision is coarser, within $\pm 2^{\circ}\text{C}$.

Load Frame and Triaxial Cell.-- A load frame capable of delivering 220 kips at a displacement rate of 1 in/sec has been specified. The frame can also have vertical stress control. The triaxial cell will be designed for a maximum confining pressure of 11000 psi. The confining stress will be applied in fixed proportion to the vertical axial stress. This requires strain control of axial loading with a second loop to adjust the confining pressure.

Acoustic Emission Monitoring System.-- The system will be capable of performing three-dimensional location analysis of microcracks using six resonant transducers located around a cylindrical specimen. Transducers should have a resonant frequency of about 0.2 MHz and a frequency bandwidth of between 0.1 to 0.6 MHz. Discrimination time is at most 150 micro-seconds. Fast data acquisition together with the ability to dump data directly onto disk will allow for rapid data and post test analyses.

The experimental program has been designed to verify the theoretical aspects of the flow and damage models, i.e., (i) to generate a comprehensive set of experimental data at constant strain rates for characterizing the deformation of materials when damage processes are active; (ii) to investigate the formation of "first" cracks during deformation by monitoring acoustic emissions; (iii) to develop and apply quantitative acoustic emission theory for locating cracks (position, time, direction, and size); and (iv) to theoretically characterize the rate-sensitive evolution of damage during deformation by flow.

All four areas of the investigation will be carried out at low and high strain rates of loading, under uniaxial and triaxial loading conditions, and at various temperatures. The testing program should commence towards the end of year two (i.e., fall 1988).

C. LIST OF PUBLICATIONS

1. A Multiaxial Differential Flow Law for Polycrystalline Ice, Submitted to Cold Regions Science and Technology, December, 1987.
2. A Rate-Sensitive Continuum Damage Model for Ice, in preparation.

D. LIST OF PARTICIPATING SCIENTIFIC PERSONNEL

1. Professor S. Shyam Sunder, Associate Professor of Civil Engineering (Project Supervisor.)
2. Mao S. Wu, Graduate Student, Department of Civil Engineering (Research Assistant.).

4. BIBLIOGRAPHY

Ashby, M.F. and Duval, P. (1985), The Creep of Polycrystalline Ice, Cold Regions Science and Technology, 11, 285-300.

Chaboche, J.L. (1984), Anisotropic Creep Damage in the Framework of Continuum Damage Mechanics, Nuclear Engineering and Design 79, 309-319.

Costin, L.S. (1983), A Microcrack Model for the Deformation and Failure of Brittle Rock, Journal of Geophysical Research, Vol. 38, 9485-9492.

Frederking, R. (1977), Plane-Strain Compressive Strength of Columnar-Grained and Granular Snow-Ice, Journal of Glaciology, Vol. 18, No. 80, 505-516.

Glen, J.W. (1955), The Creep of Polycrystalline Ice, Proceedings of the Royal Society of London, Ser. A, Vol. 228, No. 1175, 519-538.

Jacka, T.H. (1984), The Time and Strain Required for The Development of Minimum Strain Rates in Ice, Cold Regions Science and Technology, 8, 261-268.

Jones, S.J. (1982), The Confined Compressive Strength of Polycrystalline Ice, Journal of Glaciology, 28, 171-177.

Jordaan, I.J. (1986), Numerical and Finite Element Techniques in Calculation of Ice-Structure Interaction, Proceedings of the IAHR Symposium on Ice, Iowa City, Iowa, Vol. II, 405-440.

Mellor, M. (1983), Mechanical Behavior of Sea Ice, U.S. Army Cold Regions Research and Engineering Laboratory, CRREL Monograph 83-1, p. 105.

Murakami, S. and Ohno, N. (1981), A Continuum Theory of Creep and Creep Damage, in Creep in Structures, A.R.S. Ponter (Ed.), Springer-Verlag, 422-443.

Murakami, S., Sanomura, Y. and Saitoh, K. (1986), Formulation of Cross-Hardening in Creep and Its Effect on the Creep Damage Process of Copper, ASME Journal of Engineering Materials and Technology, Vol. 108, 167-173.

Sinha, N.K. (1978), Rheology of Columnar-Grained Ice, Experimental Mechanics, 18(12), 464-470.

Sinha, N. K. (1979), Grain-Boundary Sliding in Polycrystalline Materials, Philosophical Magazine A, 40(6), 825-842.

Sinha, N.K. (1981), Rate Sensitivity of Compressive Strength of Columnar-Grained Ice, Experimental Mechanics, 21(6), 209-218.

Sinha, N.K. (1982), Constant Strain- and Stress-Rate Compressive Strength of Columnar-Grained Ice, Journal of Materials Science, 17, 785-802. .

Sinha, N.K. (1984), Intercrystalline Cracking, Grain-Boundary Sliding and Delayed Elasticity at High Temperatures, Journal of Materials Science, No. 19, 359-376.

APPENDIX A

A MULTIAXIAL DIFFERENTIAL FLOW LAW
FOR POLYCRYSTALLINE ICE

A MULTIAXIAL DIFFERENTIAL FLOW LAW FOR POLYCRYSTALLINE ICE

S. Shyam Sunder and Mao S. Wu
Massachusetts Institute of Technology, Department of Civil
Engineering, Room 1-274, Cambridge, MA 02139

1. INTRODUCTION

Boundary value problems in applied ice mechanics involving multiaxial states of stress and complex loading histories, such as those encountered during ice-structure interaction, are increasingly being solved using numerical models including the finite element method (Jordaan, 1986). Constitutive models are required to characterize the ice deformation by viscoelastic flow in numerical simulations.

In problems where only "steady state" flow is of interest, an elastic - power law creep model of ice (sometimes without the elastic component) is adequate. The most widely used model of steady state or viscous flow of polycrystalline ice is Glen's power law. The multiaxial generalization of the differential model follows from conventional elasticity theory and from the rate theory of flow. The latter is based on normality of the viscous deformation-rate to a scalar valued flow potential expressed in terms of an equivalent stress measure. Palmer (1967) has derived the multiaxial law for incompressible flow of isotropic ice, while Shyam Sunder, Ganguly and Ting (1987) have presented an orthotropic model of incompressible flow.

Both the elastic and "transient" flow behavior of ice, however, are of great importance in a broad range of ice mechanics problems (Gold, 1977, Sinha et al., 1987). The most widely used flow law for ice under uniaxial loading is the creep compliance function proposed by Sinha (1978, 1979). This formulation postulates that grain boundary sliding governs transient deformation, and that the compliance function is linearly dependent on stress and nonlinearly dependent on time. For conditions other than constant stress creep, monotonically increasing stress in particular, Sinha (1983) has applied the nonlinear compliance function in conjunction with a convolution

integral to predict the mechanical behavior. This integral formulation assumes a particular generalization of Boltzmann's superposition principle for transient deformations.

Le Gac and Duval (1980) have proposed multiaxial constitutive relations for the inelastic deformation of polycrystalline ice which account for the phenomena of isotropic and kinematic hardening. Considering deformation mechanisms in ice, Ashby and Duval (1985) have subsequently developed a kinematic hardening model based on a two-bar truss analogy. They have used the model to identify certain dimensionless variables from which a single master curve can be developed for the creep of polycrystalline ice. The appropriateness of the variables has been demonstrated using the comprehensive experimental data of Jacka (1984) for dense isotropic polycrystals with a mean grain size of 1.7 mm. The predictive capability of their model, however, has not been explicitly tested against this data set.

This paper presents a differential flow model for the deformation of polycrystalline ice which (i) accounts for both isotropic and kinematic hardening, and (ii) satisfies the dimensional requirements identified by Ashby and Duval (1985). Flow (or creep) is modeled in terms of two nonlinear deformation-rate mechanisms: the first mechanism governs the transient deformation-rate (creep) which decays to zero as both an elastic back stress and a drag stress measure increase asymptotically; the second mechanism, which is modeled in terms of the well-known power law, governs the viscous deformation-rate. The evolution of the back or rest stress contributes to kinematic hardening, while that of the drag stress contributes to isotropic hardening.

In general, numerical integration of the governing equations is necessary for predicting the model response under arbitrary loading histories since both isotropic and kinematic hardening are history dependent phenomena. However, closed form analytical solutions are available for the creep compliance function and the recovery response if only kinematic hardening is considered. When both types of hardening are included, the differential model

follows creep data on ice quite well, specifically those of Jacka (1984). Predictions of the ratio of transient (delayed elastic) strain to total strain agree qualitatively with Sinha's (1979) model if grain size effects are taken into account.

The multiaxial generalization of the differential model follows from conventional elasticity theory and from the rate theory of flow. This eliminates the need for an integral formulation under variable loading histories or multiaxial loading and for generalizing the superposition assumption for nonlinearly viscoelastic materials. Equations are derived for an orthotropic model of incompressible flow and for estimating model parameters from uniaxial experimental data.

2. UNIAXIAL DIFFERENTIAL MODEL

Physical Basis of Deformation Model.-- There is general agreement, based on theoretical and experimental work, that at least two thermally activated deformation systems, a soft system and a hard system, are present during the flow of fresh-water polycrystalline ice (Sinha, 1979, Ashby and Duval, 1985.) They may be either grain boundary sliding (with diffusional accommodation) and basal slip or basal slip and slip on a non-basal plane. A combination of these processes could be present as well.

Initially, the solid resists the applied stresses in an elastic manner and then flow begins on the soft and hard systems. However, flow, particularly on the easy soft system, causes the build-up of internal elastic stresses. This may occur as a result of grain boundary sliding next to grains poorly aligned for deformation or dislocation pile-ups at the boundaries of such grains. Dislocation pile-ups at grain boundaries have been observed in ice through scanning electron microscopy (Sinha, 1987.) The internal elastic stresses, termed back or rest stresses, resist flow. In addition, internal drag stresses which resist dislocation fluxes are generated in annealed materials undergoing flow. The increase in drag stresses are the outcome of creep resistant substructures, i.e., subgrains and cells, formed

by grain boundary sliding or dislocation movement and of dislocation entanglement, dipole formation and kink band formation during slip (particularly on the basal plane.)

A detailed understanding of evolving structural and stress states on the deformation of polycrystalline materials is unavailable at the present time. For example, only recently has an attempt been made to model the primary creep process resulting from sub-cell formation using sub-cell size and misorientation as state variables (Derby and Ashby, 1987.) However, it is well known that an increasing drag stress contributes to isotropic hardening, while an increasing rest stress contributes to kinematic hardening. In isotropic hardening, material properties are independent of the direction of straining. On the other hand, kinematic hardening induces directionally dependent material properties, referred to as deformation or stress-induced anisotropy. The Baushinger effect in metals is an example of kinematic hardening.

In this paper, the deformations resulting from the interactions between the soft and hard systems are decomposed into two components; a transient flow component and a steady flow component. Steady state flow, representing a balance between work-hardening and recovery, is associated with viscous (irrecoverable) strains. Isotropic and kinematic hardening phenomena are active during transient flow and give rise to elastic strains. These strains are recoverable on unloading since equilibrium requires the internal elastic back stress to reduce to zero. The time-dependent elastic strains defining transient deformation represent the phenomenon of delayed elasticity or anelasticity.

Mathematical Formulation.-- The governing equation for the model under uniaxial conditions is obtained by expressing the total strain rate as a sum of its components, i.e.:

$$\dot{\epsilon} = \dot{\epsilon}_e + \dot{\epsilon}_t + \dot{\epsilon}_v \quad (1)$$

where the three terms on the right hand side, representing

instantaneous elasticity, transient flow and steady state or viscous flow are described in what follows.

The instantaneous elastic strain, ϵ_e , is related to the stress, σ , through the Young's modulus, E , of polycrystalline ice; this relationship may be expressed in rate form as:

$$\dot{\epsilon}_e = \dot{\sigma}/E \quad (2)$$

Several investigators (see, e.g., Gold, 1977) have shown using high-frequency sonic methods that the Young's modulus of polycrystalline fresh-water ice varies in the range of 9-11 GPa, with negligible temperature dependence between -5°C and -45°C .

The viscous strain, ϵ_v , which is associated with secondary creep or steady flow conditions, follows the well known Norton type power law of Glen (1955), i.e.,

$$\dot{\sigma} = V \dot{\epsilon}_v^{1/N} \quad (3)$$

where N is the power law index and V is a temperature dependent constant characterized by an Arrhenius activation energy law:

$$V = V_0 \exp(Q/NRT) \quad (4)$$

T is the temperature in Kelvin, V_0 is a temperature independent constant, Q is the activation energy, and R is the universal gas constant equal to $8.32 \text{ J mol}^{-1} \text{ K}^{-1}$. The activation energy for steady flow of columnar-grained polycrystalline ice has been experimentally determined by Gold (1973) to be 65 KJ mol^{-1} for temperatures in the range of -5°C to -40°C . While the activation energy for pure single crystals does not change with temperature up to -0.2°C , Gold (1983) suggests that Q varies at the higher temperatures for polycrystalline ice and that at temperatures greater than -5°C it is probably closer to 100 KJ mol^{-1} . Similar trends have been observed by Barnes et al. (1971.)

The transient strain rate $\dot{\epsilon}_t$ is taken to follow a Norton

type power law driven by a reduced stress measure, σ_r , i.e.,

$$\dot{\epsilon}_t = (\sigma_r/V)^N = \left[\frac{\sigma - R}{BV} \right]^N \quad (5)$$

where the variable R represents the back stress and B is a non-dimensional drag stress. Implicit in the formulation of Eq. (5) are the assumptions that: (i) the exponent N is the same as that for steady flow in Eq. (2), and (ii) the temperature dependence of the transient deformation-rate, represented by the parameter V , is given by an Arrhenius law with an activation energy equal to that for steady flow. For columnar-grained polycrystalline (fresh-water) ice the former assumption can be deduced from the numerical values for parameters in Sinha's (1978) time-hardening model, and for dense isotropic polycrystals from the strain-hardening model of Ashby and Duval (1985). Sinha (1978) has also shown that the activation energy for transient flow is equal to 67 KJ mol^{-1} , which agrees well with Gold's (1973) data for steady flow in the same type of ice.

Evolution equations must be specified for R and B which are history-dependent variables representing transient flow. Since the transient strains are elastic in nature, the time rates of change of the back and drag stresses are linearly proportional to the transient strain rate. The following equations are postulated to describe the evolution of R and B :

$$\dot{R} = AE \dot{\epsilon}_t \quad (6)$$

$$\dot{B} = H |\dot{\epsilon}_t| \operatorname{sgn} \left[\frac{d|\epsilon_t|}{dt} \right] \quad (7)$$

The initial value of R is zero for an annealed material or for a material that has recovered from prior loading. On the other hand the initial value of B , i.e., B_0 , may represent the annealed state of the material or some level of initial hardening introduced by pre-straining. Both A and H are temperature independent and dimensionless variables.

Under creep loading R will asymptotically increase to a

value equal to the applied stress, at which point transient flow will cease. In the case of constant strain rate loading, R approaches the steady state stress asymptotically. The maximum value of transient strain in both these cases is given by $\epsilon_{t,max} = \sigma/AE$ when R is zero initially. A value of A less than one suggests that this magnitude is greater than the instantaneous elastic strain. For the same loading conditions, the drag stress reaches a maximum value equal to $B_0 + H\epsilon_{t,max}$. This constraint on the maximum value of B states that the isotropic resistance to transient flow is not unbounded; if it is unbounded and approaches infinity, the material will lose its ability to undergo further flow.

Under reversed or cyclic loading R will reverse or switch back and forth between positive and negative values, i.e., the physical processes associated with kinematic hardening can locally relax or move back and forth, thus preventing a continual build-up which would lead to considerable hardening. The signum function is used in Eq. (7) to ensure that B has the same effect on material behavior under both compressive and tensile loadings. For instance, it can be inferred from Eq. (7) that $B > 0$ during both tensile and compressive creep tests, while it is negative during unloading in both types of tests. The decrease in drag stress during unloading indicates a decreasing resistance to grain boundary sliding and dislocation fluxes. This may arise from a spatial bias in the distribution of defects generated by isotropic hardening which favors regions of high back stress concentration.

Equations (1)-(7) define the governing differential equations for the uniaxial model. For creep loading, the solutions of Eqs. (1)-(4) are trivial. However, Eqs. (5)-(7) are coupled and numerical integration is necessary to compute the transient strains if both isotropic and kinematic hardening are present. If isotropic hardening is absent, i.e., B is a constant, analytical solutions can be obtained as shown in a subsequent section. For a general or variable loading history, the governing equations are all coupled and numerical integration is required.

Model Formulation in Dimensionless Variables.-- For the special cases of constant stress and constant strain rate loading, Ashby and Duval (1985) have suggested that unique relationships exist between certain dimensionless variables. Such relationships are predicted by the proposed model as shown below.

For creep of polycrystalline ice at constant applied stress, Ashby and Duval (1985) have considered the following dimensionless variables for strain, strain rate, time, and the back stress:

$$\tilde{\epsilon} = \epsilon E / \sigma \quad (8)$$

$$\tilde{t} = t / t_v \quad (9)$$

$$\tilde{t} = t \dot{\epsilon}_v E / \sigma \quad (10)$$

$$\tilde{R} = R / \sigma \quad (11)$$

Substituting Eqs. (8)-(11) in Eqs. (2), (3) and (5) yields:

$$\tilde{\epsilon}_e = 1 \quad (12)$$

$$\tilde{\epsilon}_v = \tilde{t} \quad (13)$$

and

$$\tilde{t}_v = 1 \quad (14)$$

$$R + B \tilde{t}_t^{1/N} = 1 \quad (15)$$

In order that Eq. (7) also reduces to a dimensionless form, the hardening parameter H is defined as HE/σ . The dimensionless evolution equations can then be expressed as:

$$\tilde{R} = A \tilde{t}_t \quad (16)$$

$$\frac{d\tilde{B}}{d\tilde{t}} = \tilde{H} |\tilde{t}_t| \operatorname{sgn} \left[\frac{d|\epsilon_t|}{d\tilde{t}} \right] \quad (17)$$

In the above equations the differentiation is with respect to dimensionless time. Equations (12)-(17) show that the model predicts a unique relationship between the dimensionless

variables and is independent of applied stress level and temperature.

Under constant strain rate loading the model predicts that a unique relationship exists between dimensionless stress $\tilde{\sigma}$ and dimensionless time \tilde{t} , independent of the applied strain rate $\dot{\epsilon}_a$ and temperature. Consider the following dimensionless variables for stresses, time, and strains, as suggested by Ashby and Duval (1985):

$$\tilde{\sigma} = \frac{\sigma}{\sigma_{\min}} ; \quad \tilde{R} = \frac{R}{\sigma_{\min}} \quad (18)$$

$$\tilde{t} = \frac{t \dot{\epsilon}_a E}{\sigma_{\min}} \quad (19)$$

$$\tilde{\epsilon}_e = \frac{\epsilon_e E}{\sigma} ; \quad \tilde{\epsilon}_v = \frac{\epsilon_v E}{\sigma} ; \quad \tilde{\epsilon}_t = \frac{\epsilon_t E}{\sigma} \quad (20)$$

where σ_{\min} is the stress corresponding to the minimum creep rate given by Glen's power law, Eq. (3):

$$\sigma_{\min} = V \dot{\epsilon}_a^{1/N} \quad (21)$$

Substituting Eqs. (18)-(20) in Eqs. (2), (3), (5)-(7) yields:

$$\dot{\tilde{\epsilon}}_e = \frac{\dot{\tilde{\sigma}}}{\tilde{\sigma}} (1 - \tilde{\epsilon}_e) \quad (22)$$

$$\tilde{\epsilon}_v = \frac{1}{\tilde{\sigma}} [\tilde{\sigma}^N - \tilde{\epsilon}_v \dot{\tilde{\sigma}}] \quad (23)$$

$$\dot{\tilde{\epsilon}}_t = \frac{1}{\tilde{\sigma}} \left[\frac{\tilde{\sigma} - \tilde{R}}{B} \right]^N - \frac{\tilde{\epsilon}_t}{\tilde{\sigma}} \dot{\tilde{\sigma}} \quad (24)$$

$$\dot{\tilde{R}} = A \frac{d}{d\tilde{t}} [\tilde{\sigma} \tilde{\epsilon}_t] \quad (25)$$

$$\frac{dB}{d\tilde{t}} = \tilde{H} \left| \frac{d}{d\tilde{t}} [\tilde{\sigma} \tilde{\epsilon}_t] \right| \operatorname{sgn} \left[\frac{d|\tilde{\epsilon}_t|}{d\tilde{t}} \right] \quad (26)$$

where $\dot{\tilde{\sigma}}$ indicates $d\tilde{\sigma}/d\tilde{t}$, and similarly for $\dot{\tilde{t}}_e$, $\dot{\tilde{t}}_v$, $\dot{\tilde{t}}_t$, and $\dot{\tilde{R}}$. Upon substituting Eqs.(22)-(24) in Eq. (1) expressed in dimensionless form, the following equation is obtained:

$$\dot{\tilde{\sigma}} = 1 - \left[\tilde{\sigma}^N + \left[\frac{\tilde{\sigma} - \tilde{R}}{B} \right]^N \right] \quad (27)$$

Eqs. (24)-(27) can be integrated with the initial conditions of zero dimensionless stress and transient strain. As steady state is reached, i.e., the dimensionless stress rate and transient strain rate decay to zero, the above equations show that the dimensionless stress and transient strain tend to one and $1/A$, respectively. The stress at steady state will therefore attain the value of σ_{min} given by Eq. (21). A single master curve can be used to relate the dimensionless stress and time since the temperature dependent constant V and the applied strain rate have been eliminated from the equations. Experimental data is currently unavailable for verifying the dimensionless relationships under constant strain rate loading.

Closed-Form Analytical Solutions for Creep and Recovery Response.-- As previously stated, closed form analytical solutions exist for creep and recovery response when isotropic hardening is absent, i.e., B is a constant. These solutions are valuable since they provide insights regarding the behavior of the model. The analytical solutions are derived below.

In an ideal creep test the stress, σ , is applied instantaneously and the stress rate history is a Dirac delta function, $\delta(t)$, with amplitude σ . This history is zero for all t except at $t=0$ where it is infinity such that:

$$\int_{-\infty}^{t^*} \sigma \delta(t) dt = \sigma \quad (28)$$

for $t^* > 0$ and zero otherwise. Consequently, the initial strain rate predicted by the model is also a Dirac delta function, i.e.,

it is equal to infinity. The amplitude of this function is σ/E , which when integrated in a manner similar to Eq. (28) corresponds to the instantaneous elastic strain. For time incrementally greater than zero, the strain rate is finite and equals:

$$\dot{\epsilon}^+ = (\sigma/BV)^N + (\sigma/V)^N \quad (29)$$

Equation (29) recognizes that the elastic back stress in Eq. (5) is equal to zero initially. Since the first term of the equation which represents transient flow dominates the initial creep response, the constant B will generally be less than one.

The dimensionless creep compliance function for the model, J, is the sum of the dimensionless elastic, transient and viscous strains, respectively, i.e.

$$J = \tilde{\epsilon}_e + \tilde{\epsilon}_t + \tilde{\epsilon}_v \quad (30)$$

The dimensionless elastic and viscous strains are given in Eqs. (12) and (13). The dimensionless transient strain can be analytically derived from Eqs. (15) and (16) with a substitution of variables approach. In particular, define a variable q as follows:

$$q = 1 - A \tilde{\epsilon}_t \quad (31)$$

Then,

$$\dot{q} = -A \tilde{\epsilon}_t \quad (32)$$

Substitution of Eqs. (31) and (32) into Eq. (15) and a separation of variables yields:

$$\int \frac{dq}{q^N} = \frac{-A}{B^N} \int d\tilde{t} \quad (33)$$

Integrating Eq. (33), applying the initial condition of $\tilde{\epsilon}_t = 0$, i.e., $q = 1$, and substituting for q results in:

$$\bar{\epsilon}_t = 1/A - [A^{N-1} + A^N/B^N(N-1)t]^{1/(1-N)} \quad (34)$$

Equation (30) together with Eqs. (12), (13) and (34) provide a closed form analytical solution for the dimensionless creep compliance function. Also, by substituting Eq. (34) in Eq. (15), the dimensionless transient strain rate can be expressed in terms of dimensionless time as:

$$\dot{\bar{\epsilon}}_t = [B^{N-1} + A/B(N-1)\bar{\epsilon}]^{N/(1-N)} \quad (35)$$

Equations (34) and (35) show that the dimensionless transient strain and strain rate tend to $1/A$ and $1/B^N$ as dimensionless time tends to infinity and zero, respectively.

If creep recovery is allowed to occur at time $t=t_u$, the elastic component of the strain is recovered instantaneously while the viscous component is irrecoverable and remains unchanged with time. However, the transient strain will decay with time according to the following closed form analytical solution that can be derived from Eqs. (15) and (16) in a manner similar to Eq. (34):

$$\bar{\epsilon}_t = [\bar{\epsilon}_{tu}^{1-N} + (A/B)^N(N-1)(t-t_u)]^{1/(1-N)} \quad (36)$$

where $\bar{\epsilon}_{tu}$ is the dimensionless transient strain at the time of unloading. Equation (36) shows that the dimensionless transient strain decays to zero with dimensionless time after unloading.

3. EXPERIMENTAL VALIDATION OF UNIAXIAL MODEL

This section first identifies the uniaxial model parameters and discusses methods for determining them. Then, model predictions under constant stress loading are verified against the experimental data of Jacka (1984) and Sinha (1978). The model is also compared with Sinha's (1979) predictions for the relative contribution of transient strain to the total strain during creep. To further demonstrate the capability of the model, the predicted strain response under a monotonically increasing stress

history is verified against Sinha's (1981) test data. Finally, the creep and recovery response of randomly oriented snow ice is studied using Brill and Camp's data taken from Sinha (1979).

Parameter Identification and Estimation.-- The uniaxial model contains a total of six parameters: E , N , V_0 , A , H and B_0 . For single ice crystals and transversely isotropic ice, five independent elastic moduli are needed to describe elastic behavior. Values for these elastic moduli are available for single crystals (see for example, Green and Mackinnon, 1956). The value of E for polycrystalline isotropic ice can be estimated fairly well from the elastic moduli of single crystals (Gammon et al., 1983). Typical values of E for isotropic polycrystalline ice are given in Section 2 of this paper.

Based on the results of tests by a number of researchers carried out at -10°C in the stress range 0.1 to 2 MPa, Ashby and Duval (1985) have estimated the value of N to be three for the creep of isotropic polycrystals and two for the basal glide of monocrystals. The use of $N=3$ for isotropic polycrystalline ice at moderate stresses is supported by theoretical models which assume dislocation mobility as the rate-controlling process (Baker, 1982). Sinha (1978) has also suggested the same value for the stress exponent in his equation for the viscous creep of polycrystalline ice.

The temperature independent constant V_0 and the activation energy Q can be estimated from creep data for various temperatures. From the values of the parameters used in Sinha's equation (1978, 1979), V_0 is estimated to be $6.59 \times 10^{-3} \text{ MPa s}^{1/N}$ for $Q=67 \text{ KJ mol}^{-1}$.

Under constant stress loading, the parameters A and B_0 determine the maximum value of the transient strain (σ/AE) and the initial transient strain rate $(\sigma/B_0V)^N$, respectively. The constant A can be estimated by subtracting the elastic strain and the viscous strain from the total strain when steady state is reached. Since the total recoverable deformation is $\sigma/E + \sigma/AE$, the fully relaxed modulus, equal to the applied stress per unit maximum recoverable deformation, is given by $EA/(1+A)$. This

allows A to be computed from a creep recovery test as well. The constant B_0 can be estimated from Eq. (29). This requires knowledge of the initial strain rate and the constant V . The latter can be computed from Eq. (4), but initial strain rates derived from the measured initial strains may be somewhat inaccurate since experimental measurements of small strains tend to be unreliable (Jacka, 1984, Mellor and Cole, 1982). The parameter H controls the amount of isotropic hardening at a given time. It can be estimated from creep strain and strain rate data using Eq. (5). Having determined V , the viscous strain and strain rate histories are known, and the transient strains and strain rates can then be extracted from the creep data. Noting Eqs. (6) and (7), Eq. (5) can be written in the following way:

$$\ln[\sigma - AE\epsilon_t - B_0 V \dot{\epsilon}_t^{1/N}] = \ln H + \ln [V \epsilon_t \dot{\epsilon}_t^{1/N}] \quad (37)$$

The quantity on the left-hand side plotted against the second term on the right-hand side of Eq. (37) is a straight line and H can be computed from its intercept with the y-axis.

Comparisons of the model predictions with experimental data in this paper is based on the following values for N , E , V_0 and Q :

$$\begin{aligned} N &= 3 \\ E &= 9500 \text{ MPa} \\ V_0 &= 6.59 \times 10^{-3} \text{ MPa s}^{1/N} \\ Q_0 &= 67 \text{ kJ mol}^{-1} \end{aligned}$$

Comparison of Model Predictions with Jacka's Creep Data.--

Jacka (1984) has published results of uniaxial compression tests on isotropic polycrystalline ice with a mean grain size of 1.7 ± 0.2 mm. The samples were tested under constant stress ranging from 0.1 to 1.5 MPa at the following specific temperatures: -5.0 , -10.6 , -17.8 and -32.5°C . Figs. 1, 2 and 3 show plots for Jacka's data (taken from Ashby and Duval, 1985) corresponding to $\bar{\epsilon}$ versus \bar{t} , $\bar{\epsilon}$ versus $\bar{\dot{\epsilon}}$, and $\bar{\dot{\epsilon}}$ versus $\bar{\epsilon}$, respectively. The predictions of the model, obtained by solving Eqs. (15)-(17) are indicated by solid lines with $A=0.017$, $B_0=0.24$ and $\bar{H}=0.024$. Also shown are the model predictions for no isotropic hardening,

i.e., solutions provided by Eqs. (12)-(14) and Eqs. (34)-(35). Parameters used for generating these curves are $A=0.033$ and $B=0.402$. Note that for experimental data plotted in dimensionless form, the model predictions using Eqs. (12)-(17) as well as Eqs. (34)-(35) are independent of E , V_0 and Q . Ashby and Duval (1985) have modified Sinha's equation for creep to a form which satisfies the dimensional requirements. The predictions of the modified equation are also shown in the figures. In referring to Jacka's data it is understood that all variables are normalized and the word dimensionless is dropped when referring to them.

The solid lines show that agreement between model predictions and data is good when strain rate is plotted against time or strain (Figs. 1 and 2). The predicted master curve in the strain versus time plot (Fig. 3) represents the data well, but at small times the predicted strains somewhat overestimate the experimental data. With no isotropic hardening, the strain rates are underestimated while the strains agree well with data. On the other hand, the modified equation provides a good prediction of the strain rate versus time response (Fig. 1), but it overpredicts the initial strains (Figs. 2 and 3) in spite of a factor of two reduction in the value of the parameter (parameter A in Ashby and Duval's paper) which equals the maximum transient strain.

Comparison of Model Predictions with Sinha's Creep Data.--

Sinha (1978) has conducted tests on the creep behavior of transversely isotropic columnar-grained ice (S-2 ice) with an average grain diameter of 3 mm. The tests were conducted in the temperature range of -9.9 to -41°C under a uniaxial compressive load of 0.49 MPa acting in the plane of transverse isotropy. Based on the observations that the activation energy for both viscous flow and transient deformation appears to be equal and that Young's modulus is relatively independent of temperature, Sinha (1978) postulated that the time dependence of the strain at one temperature can be obtained by shifting the measured dependence at another temperature along the time scale using a shift function. Figure 4 shows the creep strains obtained at

various temperatures shifted to a reference temperature of -10°C . The solid line indicates the model prediction with $A=0.33$, $B_0=0.058$ and $\tilde{H}=0.63$. The value of A is identical to that obtained by Sinha (1978).

The agreement between the experimental data and theoretical results is very good. Notice also that the values of A , \tilde{H} and B_0 used for Sinha's and Jacka's data are different, reflecting differences in the ice types that were tested, i.e., isotropic and granular versus transversely-isotropic and columnar-grained, and the average diameters of ice grains. Such modifications to parameter values are also needed for Sinha's equation. For example, the parameter corresponding to A was determined to be $1/3$ from Sinha's tests on ice with a grain size of 3 mm, but values of $1/70$ and $1/35$ were found to be suitable for Jacka's data (Ashby and Duval, 1985).

Model Prediction of Ratio of Transient to Total Strain.--

The parameter AE can be interpreted as an anelastic modulus (not to be confused with relaxed modulus), while BV represents the resistance to transient flow. If transient deformation is related to grain size as postulated by Sinha (1979), then the parameters A and H will depend on grain size. Sinha's (1979) model considers both transient strain and strain rate to be inversely proportional to grain size. For consistency with this formulation, it is necessary for the model parameters to be related to the grain size d as follows:

$$A = d/A' \quad (38)$$

$$B_0 = B_0' d^{(1/N)} \quad (39)$$

$$\tilde{H} = \tilde{H}' d^{(2/N)} \quad (40)$$

where A' , B_0' and \tilde{H}' are grain size independent material parameters. The values of these latter parameters are calculated from Eqs. (38)-(40) respectively. For the previously determined values of A , B_0 and \tilde{H} (viz., 0.33, 0.058 and 0.63) $A'=9$ mm, $B_0'=0.04 \text{ mm}^{-1/N}$, and $\tilde{H}'=0.3 \text{ mm}^{-2/N}$.

The analytical solutions for the case of no isotropic

hardening are useful for inferring some of the characteristics of the complete model. It is apparent from Eqs. (14) and (35) that the ratio of the (dimensionless) transient strain rate to the viscous strain rate decreases with increase in grain size. The ratio also decreases with dimensionless time (Eq. 35). According to the definitions of dimensionless time (Eq. (10)) and viscous strain rate (Eq. (3)), the ratio must also decrease with increase in applied stress. These trends are in agreement with predictions of Sinha's equation.

The predictions of the proposed model and Sinha's equation with regard to the relative contribution of transient strain to total strain are compared below. Let the ratio of the transient strain to the total strain, γ , be defined as follows:

$$\gamma = \frac{\tilde{\epsilon}_t}{\tilde{\epsilon}} = \frac{\tilde{\epsilon}_t}{\tilde{\epsilon}_t + \tilde{t} + 1} \quad (41)$$

where the dimensionless variables have been defined previously. By solving Eqs. (15)-(17) the strain dependence of γ under a constant stress load of 1 MPa at -10°C for various grain sizes is predicted as shown in Fig. 5. The important features predicted by Sinha's equation such as the increasing value of γ with decreasing d , the occurrence of maximum γ at small strains, the gradual shift of the maxima towards larger strains with decreasing d , the gradual decrease in γ with increase in strain after the peak is passed, and the decreasing effect of d on γ at large strains are also observed in Fig. 5, although the numerical values are different.

Furthermore, since the relationship between the dimensionless transient strain and time is independent of temperature (Eq. (34)), it can be deduced from Eq. (41) that the evolution of γ with dimensionless strain for a given grain size is unique, i.e., independent of both temperature and stress level. Recalling that dimensionless strain is equal to $\epsilon E/\sigma$ and if E does not change appreciably with temperature, then for a given grain size, the evolution of γ with strain (stress) itself

is independent of temperature but not of stress (strain). This is also predicted by Sinha's equation.

Prediction of Model Response Under Monotonically Increasing Stress.-- The rate sensitivity of the compressive strength of columnar-grained ice under constant cross-head displacement rates has been investigated by Sinha (1981). It was shown that the results are representative of the constant stress rate rather than the constant strain rate condition. A numerical integration method, based on a generalized creep equation and the principle of superposition, was developed by Sinha (1983) to predict the evolution of strain corresponding to a given stress history.

For the proposed model, the strain response can be obtained by numerically integrating Eqs. (1)-(7). In this example, the actual stress-time history (not the constant stress rate idealization) is taken as input and is known from Sinha's (1981) tests on ice with an average grain size of 4.5 mm. The tests were carried out at -10°C under a constant cross-head displacement rate of 1.25×10^{-3} cm/s. The values of the hardening parameters are determined from Eqs. (38)-(40) for the given grain size and previously determined values of the grain size independent parameters.

The stress-time data is presented in the upper curve of Fig. 6b, while the lower curve shows the predicted strain-time response superimposed on the test data. The agreement between theory and experiment is quite good, given that the parameter values which were determined from a different data set are unchanged. Figure 6a shows that when stress is plotted against strain, a very good representation of the data is obtained. It is possible to conclude from this figure that the predictions of the proposed model under monotonically increasing stress compare well with experimental data.

Comparison of Model Predictions with the Creep and Recovery Data of Brill and Camp.-- Figure (7) shows creep and recovery data for tests conducted on randomly oriented snow ice by Brill and Camp (reproduced in Sinha, 1979.) The three sets of data refer to tests carried out under the following conditions: curve

(a) at -5°C and 0.232 MPa, curve (b) at -5°C and 0.125 MPa, and curve (c) at -10°C and 0.238 MPa. The model predictions, shown in solid lines, are generated with $A'=6.5$ mm, $B_0'=0.11$ $\text{mm}^{-1/N}$ and $\bar{H}'=0.01$ $\text{mm}^{-2/N}$. The grain sizes used for curves (a), (b) and (c) are 2 mm, 2.3 mm, and 1.5 mm respectively, which are almost identical to the values determined by Sinha (1979). Differences in the hardening parameters reflect the difference in ice types, i.e., transversely isotropic and columnar-grained versus isotropic and granular snow ice. The agreement between model predictions and test data is quite good, given that the measurement of strain recovery in ice shows large scatter (Sinha, 1982.)

A major difference exists between Sinha's recovery model and the present formulation. The former can result in a decrease of the permanent/irrecoverable viscous strain and eventually lead to reversed strain (e.g., an elongation or tensile strain due to recovery from compressive creep). This is due to the particular form of the superposition principle adopted, in which the elastic and the transient strains resulting from the stress drop are subtracted from the total strain at unloading. Recovery is thus the mirror image of the transient term in the equation for loading and as time increases it can exceed the transient creep strain at the instant of unloading. In order to overcome the problem, the superposition principle is not used when the predicted strain during recovery becomes less than the accumulated viscous strain and the strain is kept fixed thereafter at a value equal to that of the viscous strain at unloading. The proposed theory does not suffer from this modeling limitation since the values of R and B decrease during unloading, reflecting creep recovery.

4. MULTIAXIAL MODEL FORMULATION

Natural ice has very complex crystalline and stratigraphic structures, and generally cannot be considered as an isotropic material. For example, columnar fresh-water ice may have two sources of anisotropy: (a) the c -axis may be oriented

perpendicular to the axis of crystal growth, and (b) the c-axes of different crystals may show preferred orientation in the plane on which they lie. According to the classification of Michel and Ramseier (1971), the first source of anisotropy is exhibited by S2 ice while both types of anisotropy are present in S3 ice.

The anisotropy of ice strongly influences its mechanical behavior. Carter and Michel (1971) have tested S2 ice at -10°C under constant strain rate loading conditions. They find that the first source of anisotropy leads to a vertical to horizontal maximum stress or strength ratio of about two. Information on the effect of the second source of anisotropy on the strength ratio of freshwater ice is currently unavailable, although data for sea ice indicates the following strength ratios: (a) 0.25-0.60 for strength at a 45 degree azimuthal angle to that along the c-axes, and (b) 0.50-0.95 for strength at a 90 degree angle to that along the c-axis (Peyton, 1968; Vittoratos, 1979; Wang, 1979; Richter-Menge et al., 1985).

Theoretical formulations which account for anisotropy in ice with a transversely isotropic model have been developed by Reinicke and Ralston (1977) and by Vivatrat and Chen (1985). The former model is based on plasticity theory and considers ice to be a pressure sensitive material as well. The latter is a pressure insensitive, elastic - power law creep formulation.

The development presented here is based on an orthotropic generalization (i.e., the general case of a material having three orthogonal planes of symmetry) of the proposed uniaxial model which accounts for both transient and steady state flow in ice. The transversely isotropic and isotropic formulations are special cases of the orthotropic generalization.

Conceptual Framework and Constraint Conditions.-- The three-dimensional generalization of the model follows naturally from the uniaxial formulation, i.e., it is based on strain decomposition, linear elasticity and the rate theory of flow. Constitutive relations are derived for each mechanism of deformation in the model, resulting in the orthotropic equivalent of Eqs. (1)-(7).

To model orthotropic elasticity, the classical formulation from elasticity theory is adopted (see, for example, the book by Lekhnitskii, 1963). Compressibility of ice deformation is implicitly contained in linear elasticity where the Poisson's ratios are less than 0.5, while the transient and viscous deformation-rate mechanisms are assumed to be incompressible (Palmer, 1967, Sinha, 1987). The orthotropic generalization of the viscous deformation-rate mechanism is derived from the rate theory of flow by applying the normality principle to a scalar valued flow potential expressed in terms of an equivalent stress measure for incompressible orthotropic materials. Similarly, the derivation of the orthotropic constitutive relations for transient flow are based on the normality of the stress difference vector $\underline{\sigma} - \underline{R}$ to a scalar valued flow potential expressed in terms of an equivalent stress difference measure. Evolution equations for the back stress vector \underline{R} and the equivalent drag stress B_{eq} follow from the uniaxial equations.

The total, elastic, viscous and transient strain rate vectors must obey the following constraint condition:

$$\dot{\underline{\epsilon}} = \dot{\underline{\epsilon}}_e + \dot{\underline{\epsilon}}_v + \dot{\underline{\epsilon}}_t \quad (42)$$

where the strain rates are in engineering notation, for example, $\dot{\underline{\epsilon}} = [\dot{\epsilon}_{xx} \ \dot{\epsilon}_{yy} \ \dot{\epsilon}_{zz} \ \dot{\gamma}_{xy} \ \dot{\gamma}_{yz} \ \dot{\gamma}_{zx}]^T$. The superscript T denotes the transpose of vectors and matrices. For convenience, the stress difference $\underline{\sigma} - \underline{R}$ is denoted by the symbol $\underline{\sigma}_d$, i.e.:

$$\underline{\sigma}_d = \underline{\sigma} - \underline{R} \quad (43)$$

The stress vectors are also expressed in engineering notation.

Orthotropic Model of Elasticity.-- The constitutive relation between the elastic strain and the stress is described in rate form as:

$$\dot{\underline{\epsilon}}_e = \underline{C} \dot{\underline{\sigma}} \quad (44)$$

where \underline{C} is the compliance matrix for a linearly elastic but

orthotropic material. Values of the Young's moduli, Poisson's ratios and shear moduli for orthotropic and transversely isotropic polycrystalline ice are not readily available. However, engineering approximations involving a weighted average of the five elastic constants for single crystals have been developed (Gammon et al., 1983, Ashton, 1986). The Poisson's ratio for isotropic polycrystalline ice is approximately 0.3 (Gold, 1977).

Orthotropic Model of Viscous Flow.-- To derive the relationship between the viscous strain rate vector $\underline{\dot{\epsilon}}_v$ and the stress vector $\underline{\sigma}$, an equivalent stress measure generalized for pressure insensitive orthotropic materials, i.e., with identical behavior in tension and compression, is defined:

$$\sigma_{eq}^2 = \frac{3}{\beta} \left[\frac{a_1}{3} (\sigma_{xx} - \sigma_{yy})^2 + \frac{a_2}{3} (\sigma_{yy} - \sigma_{zz})^2 + \frac{a_3}{3} (\sigma_{zz} - \sigma_{xx})^2 + 2a_4 \sigma_{xy}^2 + 2a_5 \sigma_{yz}^2 + 2a_6 \sigma_{zx}^2 \right] \quad (45)$$

with β chosen to be $(a_1 + a_2)$ so that $\sigma_e = \sigma_{yy}$ when the stress components are described by the vector $\underline{\sigma} = [0 \ \sigma_{yy} \ 0 \ 0 \ 0 \ 0]^T$, i.e., the y-axis is chosen as the reference direction. Equation (45) is similar in form to that used by Hill (1950) for metal plasticity and may be expressed in compact form using matrix notation as:

$$\sigma_{eq}^2 = 3/\beta \ \underline{\sigma}^T \underline{G} \ \underline{\sigma} \quad (46)$$

where

$$\underline{G} = \begin{bmatrix} \frac{a_1+a_3}{3} & \frac{-a_1}{3} & \frac{-a_3}{3} & 0 & 0 & 0 \\ & \frac{a_1+a_2}{3} & \frac{-a_2}{3} & 0 & 0 & 0 \\ & & \frac{a_2+a_3}{3} & 0 & 0 & 0 \\ & & & 2a_4 & 0 & 0 \\ & & & & 2a_5 & 0 \\ & & & & & 2a_6 \end{bmatrix} \quad (47)$$

SYMMETRIC

The viscous strainrate vector can now be related to the stress vector by defining a scalar valued viscous flow potential function:

$$\phi_v = a \frac{\sigma_{eq}^{N+1}}{N+1} \quad (48)$$

which obeys the normality principle:

$$\underline{\dot{\epsilon}}_v = \frac{\partial \phi_v}{\partial \underline{\sigma}} \quad (49)$$

The parameter a in Eq. (48) is a constant associated with the power law for uniaxial loading in the y -direction; it is equivalent to the quantity $1/V^N$ in Eq. (3). Combining Eqs. (46)-(49) yields the desired relationship:

$$\underline{\dot{\epsilon}}_v = \lambda \underline{S}^* \quad (50)$$

where

$$\lambda = 3/\beta \ a \ \sigma_{eq}^{N-1} \quad (51)$$

and

$$\underline{S}^* = \underline{G} \underline{\sigma} \quad (52)$$

Note that \underline{S}^* is a pseudo-deviatoric stress vector for orthotropic materials. If a_1 to $a_6 = 1$, \underline{S}^* reduces to the conventional deviatoric stress vector, σ_{eq} reduces to the conventional equivalent stress measure for isotropic materials, and Eq. (50) becomes the well known three-dimensional generalization of the power law for creep of isotropic materials, as presented by Palmer (1967) for glacier flow.

Using the hypothesis of energy equivalence, the relationship between the equivalent stress defined in Eq. (45) and an equivalent strain rate measure can be established. The rate of dissipation of energy per unit volume, P , is given by:

$$P = \underline{\sigma}^T \underline{\dot{\epsilon}}_v \quad (53)$$

Application of this hypothesis yields:

$$\underline{\sigma}^T \underline{\dot{\epsilon}}_v = \sigma_{eq} \dot{\epsilon}_{v,eq} \quad (54)$$

where $\dot{\epsilon}_{v,eq}$ is the equivalent viscous strainrate. The viscous strain rate vector in Eq. (54) can be eliminated using Eqs. (50), (52) and (46) in succession to yield:

$$\dot{\epsilon}_{v,eq} = a \sigma_{eq}^N \quad (55)$$

Given the equivalent stress measure, Eq. (55) can be used to compute the equivalent viscous strain rate. Alternatively, an explicit expression can be derived by first eliminating $(\sigma_{xx} - \sigma_{yy})^2, \dots, \sigma_{zx}^2$ in Eq. (45) through the use of Eq. (50) and then substituting the resulting expression for σ_{eq} in Eq. (55). The final expression can be expressed in compact notation as follows:

$$\dot{\epsilon}_{v,eq}^2 = \beta/3 \underline{\dot{\epsilon}}_v^T \underline{H} \underline{\dot{\epsilon}}_v \quad (56)$$

where the transformation matrix \underline{H} is given by:

$$\underline{H} = \begin{bmatrix} \frac{3(a_1+a_3)a_2^2}{a^{*2}} & \frac{-3a_1a_2a_3}{a^{*2}} & \frac{-3a_1a_2a_3}{a^{*2}} & & & \\ & \frac{3(a_1+a_2)a_3^2}{a^{*2}} & \frac{-3a_1a_2a_3}{a^{*2}} & & & \\ & & \frac{3(a_2+a_3)a_1^2}{a^{*2}} & & & \\ & & & 0 & & \\ & & & & 2/a_4 & \\ & & & & & 2/a_5 \\ & & & & & & 2/a_6 \end{bmatrix} \quad (57)$$

SYMMETRIC

with $a^* = a_2a_3 + a_3a_1 + a_1a_2$. It is apparent that Eq. (56) can be reduced to the conventional equivalent strain rate measure for isotropic materials if a_1 to $a_6 = 1$. Moreover, when loading is in the reference direction, $\dot{\epsilon}_{v,eq} = \dot{\epsilon}_{v,yy}$, and Eq. (55) reduces to uniaxial loading in the reference direction.

Orthotropic Model of Transient Flow.-- The orthotropic generalization of the transient deformation is based on the assumption of flow incompressibility. Although this may not be

strictly true, Sinha (1987) has argued that transient flow does not change the volume appreciably and that the assumption is valid. This assumption is implicitly made for metals (Hart, 1976). A second assumption is that the orthotropy is described by the same set of parameters, i.e., a_1 through a_6 .

The model accounts for isotropic hardening as well as kinematic or directional hardening, which leads to subsequent deformation or stress-induced anisotropy (as opposed to material or texture anisotropy). The relationship between the transient strain rate $\dot{\underline{\epsilon}}_t$ and the stress vector $\underline{\sigma}_d$ can be derived from the normality of $\underline{\sigma}_d$ to a scalar valued transient flow potential function. Following the procedure used to derive Eqs. (50)-(52) yields:

$$\dot{\underline{\epsilon}}_t = 3/\beta \ a/B_{eq}^N \ \sigma_{d,eq}^{N-1} \ \underline{S}_d^* \quad (58)$$

where

$$\underline{S}_d^* = \underline{G} \ \underline{\sigma}_d = \underline{G} \ \underline{\sigma} - \underline{G} \ \underline{R} \quad (59)$$

B_{eq} is the equivalent nondimensional drag stress, and $\sigma_{d,eq}^2 = 3/\beta \ \underline{\sigma}_d^T \underline{G} \ \underline{\sigma}_d$. To complete the multiaxial formulation, the evolution equations for \underline{R} and B_{eq} as well as the value of the equivalent stress difference measure are required.

For consistency with the incompressibility constraint on transient flow and the elastic nature of back stresses, it is necessary to define a scalar valued flow potential in terms of the equivalent back stress, $R_{eq}^2 = 3/\beta \ \underline{R}^T \underline{G} \ \underline{R}$, i.e.,

$$\phi_s = b/2 \ R_{eq}^2 \quad (60)$$

where b equals $1/AE$ in the reference direction. The transient strain can then be related to the pseudo-deviatoric back stress vector by imposing normality:

$$\dot{\underline{\epsilon}}_t = \frac{\partial \phi_s}{\partial \underline{R}} = \frac{3}{\beta} \ b \ \underline{S}_R^* \quad (61)$$

where

$$\underline{S}_R^* = \underline{G} \underline{R} \quad (62)$$

The evolution equation for the back stress vector is the time derivative of Eq. (61), i.e.,

$$\dot{\underline{S}}_R^* = \underline{G} \dot{\underline{R}} = \beta/(3b) \dot{\underline{\epsilon}}_t \quad (63)$$

The equivalent non-dimensional drag stress B_{eq} is given by:

$$\dot{B}_{eq} = c \dot{\epsilon}_{t,eq} \operatorname{sgn} \left[\frac{d\epsilon_{t,eq}}{dt} \right] \quad (64)$$

where c equals H in the reference direction. Both the equivalent transient strain rate and strain measures in Eq. (64) can be obtained using the transformation matrix \underline{H} , derived in Eq. (57) for the equivalent viscous strain rate.

The equivalent stress difference can be expressed as a function of the equivalent transient strain. Noting that $\sigma_{d,eq}^2$ can be defined in terms of \underline{S}_d^* as $3/\beta \underline{\sigma}_d^T \underline{S}_d^*$, and substituting $\underline{S}^* - \underline{S}_R^*$ for \underline{S}_d^* and $\underline{\sigma} - \underline{R}$ for $\underline{\sigma}_d$ yields:

$$\sigma_{d,eq}^2 = 3/\beta [\underline{\sigma}^T \underline{S}^* - 2 \underline{\sigma}^T \underline{S}_R^* + \underline{R}^T \underline{S}_R^*] \quad (65)$$

$\underline{\sigma}$ and, consequently, \underline{S}^* may be considered as given, while \underline{S}_R^* may be computed by integrating Eq. (63). Substitution of Eq. (61) in the last term of Eq. (65) yields $(\beta/3b) \underline{R}^T \underline{\epsilon}_t$, where $\underline{R}^T \underline{\epsilon}_t$ equals twice the elastic strain energy stored in the material. Based on an equivalence in the rate of stored elastic strain energy, it follows that:

$$\underline{R}^T \dot{\underline{\epsilon}}_t = R_{eq} \dot{\epsilon}_{t,eq} \quad (66)$$

The equivalent uniaxial relationship between R_{eq} and $\epsilon_{t,eq}$ is given by:

$$R_{eq} = 1/b \epsilon_{t,eq} \quad (67)$$

since $b=1/AE$. Equation (67) and the right-hand-side of Eq. (66) are integrated simultaneously with respect to time to yield $R^T \underline{\epsilon}_t$. On substitution in Eq. (65), the following result is obtained:

$$\sigma_{d,eq}^2 = 3/\beta \underline{\sigma}^T \underline{S}^* - 2/b \underline{\sigma}^T \underline{\epsilon}_t + (\epsilon_{t,eq}/b)^2 \quad (68)$$

The second term in this equation is obtained by substituting Eq. (61) in the corresponding term of Eq. (65).

Equations (42), (44), (50), (58), (63) and (64) are the orthotropic counterparts of Eqs. (1)-(3) and (5)-(7). They form the governing equations that can be integrated numerically to predict the model response under variable loading histories involving multiaxial states of stress.

5. EXPERIMENTAL VALIDATION OF MULTIAXIAL MODEL

Estimation of Orthotropic Model Parameters.-- The orthotropic model parameters can be estimated from experimental data under steady viscous flow conditions. Five uniaxial (compression) tests are required to obtain the five parameters a_2 through a_6 since a_1 can be set to one without loss of generality. In a comprehensive paper reviewing the constants used in Glen's power law for polycrystalline glacier ice, Hooke (1981) has concluded that in the absence of experimental evidence to the contrary, a value of three for the power law index N is reasonable, irrespective of the "structural state", e.g., fabric and grain size. The effect of the structural state is then accounted for by changing the "viscosity" parameter (V in the present model). This is the approach adopted here, in which N is three and the initial texture or material anisotropy is accounted for through the use of an appropriate equivalent stress measure. Under uniaxial loading in any specific direction, the viscosity parameter relating viscous strain rate and stress in the specified direction is provided by Eq. (55), the definition for the equivalent stress in Eq. (45), and the definition for the equivalent viscous strain rate in Eq. (56).

The x-axis is taken to be normal to the ice sheet which is defined by the y-z plane. The c-axes of the ice crystals are assumed to lie in the y-z plane and are aligned in the y-direction. The tests are conducted in three orthogonal directions y, x, and z respectively, and along the three 45° axes on the y-z, x-y, and z-x planes respectively. Let β_1 to β_5 represent the experimentally determined ratios of the maximum stresses (strengths) for the latter five tests, respectively, to the maximum stress in the reference y-direction for tests conducted at the same constant strain rate. In the case of creep tests, the β 's represent inverse ratios of the corresponding minimum strain rates raised to the power of $1/N$. The parameters a_2 to a_6 may be determined from the following equations (see Appendix A for derivations):

$$a_2 = - \frac{\beta_1^n - \beta_2^n (1 - \beta_1^n)}{\beta_1^n - \beta_2^n (1 + \beta_1^n)} \quad (69)$$

$$a_3 = - \frac{\beta_1^n + \beta_2^n (1 - \beta_1^n)}{\beta_1^n - \beta_2^n (1 + \beta_1^n)} \quad (70)$$

$$a_4 = \beta/6 [4\beta_4^{-n} - \beta_2^{-n}] \quad (71)$$

$$a_5 = \beta/6 [4\beta_3^{-n} - \beta_1^{-n}] \quad (72)$$

$$a_6 = \beta/6 [4\beta_5^{-n} - 1] \quad (73)$$

where $n=2N/(N+1)$. Typical values for β_1 lie between 2-5. While the values of the constants β_2 to β_5 are not generally available in the literature for pure polycrystalline ice, they may be estimated from the sea ice data referred to in the beginning of Section 4.

For a transversely isotropic material, i.e., isotropy in the y-z plane, $\beta_2=\beta_3=1$ and $\beta_4=\beta_5$. As a result, $a_1=a_3=1$, $a_4=a_6$, the parameters a_2 and a_5 are functions of only β_1 , while a_4 depends on both β_1 and β_4 . Only two uniaxial tests are required to obtain β_1 and β_4 : one in the x-direction and one along the 45° axis on the x-y or z-x planes.

Model Predictions Under Steady State Plane-Strain and Triaxial Compressive Loadings.-- Experimental data on the pure flow (both transient and steady state) of polycrystalline ice under multiaxial states of stress is unavailable, although the incompressible and isotropic power law of Palmer (1967) is widely used to describe the deformation of glacier ice under such stresses. In spite of data limitations, an attempt is made here to evaluate model predictions under steady flow conditions.

Frederking (1977) has conducted plane strain uniaxial compression tests on columnar-grained transversely isotropic freshwater ice. For his type A tests, strains in the z-direction are constrained to zero and stresses are applied in the y-direction. At steady state where the power law orthotropic formulation suffices, the ratio Γ_z of the plane strain stress to the unconfined stress at the same strain rate is directly related to β_1 by the following equation (see Appendix B)

$$\Gamma_z = \left[\frac{4\beta_1^{2n}}{4\beta_1^n - 1} \right]^{1/n} \quad (74)$$

The equation predicts Γ_z to vary between 2.1-5.1 for experimentally observed values of β_1 ranging from 2 to 5, and $N=3$. This is consistent with Frederking's experimental observations which were close to 2 at high strain rates and to 5 at low strain rates. In his type B tests, strains in the x-direction are constrained to zero while stresses are again applied in the y-direction. In this case, the ratio Γ_x is given by:

$$\Gamma_x = \left[1 + \frac{1}{4\beta_1^n - 1} \right]^{1/n} \quad (75)$$

Since β_1 is generally greater than one, Γ_x will be less than approximately 1.2 for $N=3$. For typical values of β_1 , the predicted values of Γ_x lies between 1.01 to 1.06. This is consistent with Frederking's experiments which showed negligible influence of x-direction confinement on stresses. Although the

derivation in Appendix B determines Γ_z and Γ_x as the ratios of two steady state stresses resulting from viscous flow, considerable damage occurred in Frederking's tests. The accuracy of the predictions are interesting nonetheless. This probably occurs because both the unconfined and partially confined strengths are reduced by damage, and the resulting effect on strength ratios is less significant.

According to the orthotropic model, the ratio Γ_t of the maximum axial stress with a confining pressure equal to τ times the axial stress to the maximum axial stress in the unconfined state at the same strain rate should be given by (see Appendix C):

$$\Gamma_t = \frac{1}{1-\tau} \quad (76)$$

The shear stress (i.e. axial stress minus radial stress) normalized by the unconfined stress is independent of τ or confining pressure for the model and equal to one. The triaxial behavior of pure (non-saline) polycrystalline ice has been studied by Jones (1978). His tests, which were performed at strain rates of 10^{-6} to 5×10^{-3} s $^{-1}$, indicate up to a factor of two increase in shear stress due to confining pressure. Nadreau and Michel (1986) have reported triaxial tests on freshwater, iceberg and saline ice, and their results confirm that shear strength increases with confining pressure and strain rate. The pressure and strain rate sensitivity of damage in ice, which causes the increase in shear strength with confining pressure and strain rate, is examined in the forthcoming paper by Wu and Shyam Sunder (1988).

6. CONCLUSIONS

This paper presents a multiaxial differential flow law for polycrystalline ice which attempts to model the underlying physical deformation mechanisms active in the material. Instantaneous elasticity is modeled by the classical theory of

linear elasticity, while the steady viscous deformation-rate mechanism is described by Glen's power law. On the other hand, the transient deformation-rate mechanism is modeled by the interaction between the soft and hard deformation systems which gives rise to an internal drag stress and a back stress. Increasing drag and back stresses are associated with the phenomena of isotropic and kinematic hardening, respectively. Dimensional requirements identified by Ashby and Duval (1985) are satisfied by the model.

The multiaxial generalization follows from conventional elasticity theory and from the rate theory of flow for the viscous and transient deformation-rates. The rate theory assumes normality of the deformation-rate to a scalar valued flow potential expressed in terms of an equivalent stress measure. History effects are modeled with a hardening multiaxial formulation based on the elastic back stress vector and an equivalent (scalar) drag stress measure. Equations are derived for an orthotropic model of incompressible flow and for estimating the orthotropic parameters from uniaxial test data.

The uniaxial model contains a total of six parameters that can be determined from conventional experimental testing methods for ice. The model is verified against Jacka's (1984), Sinha's (1978), and Brill and Camp's test data on the creep of polycrystalline ice. Predictions of the ratio of transient to total strain agree qualitatively with Sinha's equation if grain size effects are taken into account. The mechanical behavior under monotonically increasing stress is successfully predicted using Sinha's (1983) data obtained from constant displacement rate tests.

For the multiaxial model, experimental verification is made difficult by the lack of data for the pure flow of freshwater polycrystalline (S2 or S3) ice. The model predicts pressure-insensitive behavior under conventional triaxial loading conditions. Also, theoretical predictions agree well with Frederking's (1977) data from constant strain rate tests carried out under plane strain conditions (although it should be noted

that his data is for ice with distributed cracks or damage induced by loading, not pure flow.)

7. ACKNOWLEDGEMENTS

The authors would like to acknowledge financial support from the U.S. Army Research Office through MIT's Center for Advanced Construction Technology; EP America through MIT's Center for Scientific Excellence in Offshore Engineering; and the U.S. Department of the Interior, Minerals Management Service.

REFERENCES

- Ashby, M.F. and Duval, P. (1985), The Creep of Polycrystalline Ice, Cold Regions Science and Technology, 11, 285-300.
- Baker, R.W. (1982), A Flow Equation for Anisotropic Ice, Cold Regions Science and Technology, 6, 141-148.
- Barnes, P., Tabor, D., and Walker, J.C.F. (1971), The Friction and Creep of Polycrystalline Ice, Proceedings Royal Society London A, 324, 127-155.
- Carter, D. and Michel, B. (1971), Laws and Mechanisms of Apparent Brittle Fracture of River and Lake Ice (In French), Faculte des Sciences, Universite Laval, Quebec, Report S-22.
- Derby, B. and Ashby, M.F. (1987), A Microstructural Model for Primary Creep, Acta Metallurgica, Vol. 35, No. 6, 1349-1353.
- Frederking, R. (1977), Plane-Strain Compressive Strength of Columnar-Grained and Granular Snow-Ice, Journal of Glaciology, Vol. 18, No. 80, 505-516.
- Le Gac, H. and Duval, P. (1980), Constitutive Relations for the Non-Elastic Deformation of Polycrystalline Ice, Tryde, P. (Ed.), Proceedings of the IUTAM Symposium on the Physics and Mechanics of Ice, Springer, 51-59.
- Gammon, P.H., Kiefte, H., Clouter, M.J. and Denner, W.W., (1983), Elastic Constants of Artificial and Natural Ice Samples by Brillouin Spectroscopy, Journal of Glaciology, Vol. 29, No. 103, 433-460.
- Glen, J.W. (1955), The Creep of Polycrystalline Ice, Proceedings of the Royal Society of London, Ser. A, Vol. 228, No. 1175, 519-538.
- Gold, L.W. (1973), Activation Energy for Creep of Columnar-Grained Ice, In Whalley, E., Jones, S.J. and Gold, L.W. (Eds.), Physics and Chemistry of Ice, Roy. Soc. Canada, Ottawa, 362-364.
- Gold, L.W. (1977), Engineering Properties of Fresh Water Ice, Journal of Glaciology, Vol. 19, No. 81, 197-212.
- Gold, L.W. (1983), Creep of Columnar-Grained Ice at Low Stress, Annals of Glaciology, 4, 73-78.
- Green, R.E. and Mackinnon, L. (1956), Determination of the Elastic Constants of Ice Single Crystals by an Ultrasonic Pulse Method, Journal of the Acoustical Society of America, 28, 1292 p.
- Hart, E.W. (1976), Constitutive Relations for the Nonelastic Deformation of Metals, Journal of Engineering Materials and Technology, 96, 193-202.

Hill, R. (1950), The Mathematical Theory of Plasticity, Oxford University Press, London.

Hooke, R.L. (1981), Flow Law for Polycrystalline Ice in Glaciers: Comparison of Theoretical Predictions, Laboratory Data, and Field Measurements, Reviews of Geophysics and Space Physics, Vol. 19, No. 4, 664-672.

Jacka, T.H. (1984), The Time and Strain Required for The Development of Minimum Strain Rates in Ice, Cold Regions Science and Technology, 8, 261-268.

Jones, S.J. (1982), The Confined Compressive Strength of Polycrystalline Ice, Journal of Glaciology, 28, 171-177.

Jordaan, I.J. (1986), Numerical and Finite Element Techniques in Calculation of Ice-Structure Interaction, Proceedings of the IAHR Symposium on Ice, Iowa City, Iowa, Vol. II, 405-440.

Lekhnitskii, S.G. (1963), Theory of Elasticity of an Anisotropic Elastic Body, Holden-Day, Inc., San Francisco.

Mellor, M. and Cole, D.M. (1982), Deformation and Failure of Ice under Constant Stress or Constant Strain-Rate, Cold Regions Science and Technology, 5, 201-219.

Michel, B. and Ramseier, R.O. (1971), Classification of River and Lake Ice, Canadian Geotechnical Journal, Vol. 8, 36-45.

Miller, A. (1976), An Inelastic Constitutive Model for Monotonic, Cyclic, and Creep Deformation: Part 1 - Equations Development and Analytical Procedures, Journal of Engineering Materials and Technology, 96, 97-104.

Nadreau, J.P. and Michel, B. (1986), Secondary Creep in Confined Ice Samples, Proceedings of the IAHR Symposium on Ice, Iowa City, Iowa, Vol. I., 307-318

Palmer, A.C. (1967), Creep-Velocity Bounds and Glacier-Flow Problems, Journal of Glaciology, Vol. 6, No. 46, 479-488.

Peyton, H.R. (1968), Ice and Marine Structures, Ocean Industry, Vol. 3, No.3, March 1968, 40-41; Vol. 3, No. 9, September 1968, 59-65; Vol. 3, No. 12, December 1968, 51-58.

Reinicke, K.M. and Ralston, T.D. (1977), Plastic Limit Analysis with an Anisotropic, Parabolic Yield Function, International Journal of Rock Mechanics, Mining Sciences and Geomechanics, 14, 147-154.

Richter-Menge, J.A., Cox, G.F.N, Perron, N., Durell, G. and Bosworth, H. (1985), Triaxial Testing of First-Year Sea Ice, Internal Research Report 877, U.S. Army Cold Regions and

Engineering Laboratory, Hanover, New Hampshire.

Shyam Sunder, S., Ganguly, J. and Ting, S.K. (1987), Anisotropic Sea Ice Indentation in the Creeping Mode, Journal of Offshore Mechanics and Arctic Engineering, Vol. 109, No. 2, 211-219.

Sinha, N.K. (1978), Rheology of Columnar-Grained Ice, Experimental Mechanics, 18(12), 464-470.

Sinha, N.K. (1979), Grain-Boundary Sliding in Polycrystalline Materials, Philosophical Magazine A, 40(6), 825-842.

Sinha, N.K. (1981), Rate Sensitivity of Compressive Strength of Columnar-Grained Ice, Experimental Mechanics, 21(6), 209-218.

Sinha, N.K. (1982), Delayed Elastic Strain Criterion for First Cracks in Ice, In Vermeer, P.A. and Luger, H.J. (Eds.), Proceedings of the IUTAM Conference on Deformation and Failure of Granular Materials, A.A. Balkema Rotterdam, 323-330.

Sinha, N.K. (1983), Creep Model of Ice for Monotonically Increasing Stress, Cold Regions Science and Technology, 8, 25-33.

Sinha, N.K. (1987), Effective Poisson's Ratio of Isotropic Ice, Proceedings of the Sixth International Offshore Mechanics and Arctic Engineering Symposium, Vol. IV, 189-195.

Sinha, N.K., Timco, G.W., and Frederking, R. (1987), Recent Advances in Ice Mechanics in Canada, In Chung, J.S., Hallam, S.D., Maatanen, M., Sinha, N.K., and Sodhi, D.S. (Eds.), Advances in Ice Mechanics - 1987, ASME, Offshore Mechanics and Arctic Engineering Symposium Committee, Houston, Texas, 15-35.

Vivatrat, V. and Chen, V.L. (1985), Ice Load Prediction with the Use of a Rate-Dependent Anisotropic Law, Proceedings of the ASCE Specialty Conference: Arctic '85- Civil Engineering in the Arctic Offshore, San Francisco, California, 942-952.

Vittoratos, E.S. (1979), Existence of Oriented Sea Ice by the Mackenzie Delta, Proceedings of the 5th International Conference on Port and Ocean Engineering under Arctic Conditions (POAC 79), Trondheim, Norway, Vol. 1, August, 1979, 643-650.

Wang, Y.S. (1979), Sea Ice Properties, Proceedings of the Technical Seminar on Alaskan Beaufort Sea Gravel Island Design, Exxon Company, USA, Houston, TX, October 1979.

Wu, M.S. and Shyam Sunder, S. (1988), A Rate and Pressure Sensitive Damage Model for Polycrystalline Ice, In Preparation.

APPENDIX A

Orthotropic Material Parameters ($a_1 - a_6$)A.1 Definition of Symbols

The derivation here considers only the power law creep of ice. The parameters a_1 to a_6 and β_1 to β_5 have been defined in the paper. The coefficients a , b_2 to b_6 are the constants for the uniaxial power law along the y (reference)-, x- and z-directions, and along the 45° axes on the y-z, x-y and z-x planes respectively. Thus,

$$\dot{\epsilon}_{yy} = a \sigma_{yy}^N \quad (A.1)$$

$$\dot{\epsilon}_{45(zx)} = b_6 \sigma_{45(zx)}^N \quad (A.6)$$

where $\dot{\epsilon}_{yy}, \dots, \dot{\epsilon}_{45(zx)}$ and $\sigma_{yy}, \dots, \sigma_{45(zx)}$ are the viscous strain rate and the stress components. Also, we can set the first orthotropic parameter $a_1=1$ without loss of generality.

A.2 Uniaxial Tests in the X- and Z- Directions

To derive a_2 and a_3 , we first obtain expressions for the strain rates in the x- and z-directions using Eqs. (50 - 52) and the definition for the equivalent stress (Eq. 45). Note that the stress vectors are $\underline{\sigma} = [\sigma_{xx} \ 0 \ 0 \ 0 \ 0 \ 0]^T$ and $\underline{\sigma} = [0 \ 0 \ \sigma_{zz} \ 0 \ 0 \ 0]^T$ for loading in the X- and Z- directions, respectively. Thus:

$$\dot{\epsilon}_{xx} = a \left(\frac{1+a_3}{1+a_2} \right)^{(N+1)/2} \sigma_{xx}^N \quad (A.7)$$

$$\dot{\epsilon}_{zz} = a \left(\frac{a_2+a_3}{1+a_2} \right)^{(N+1)/2} \sigma_{zz}^N \quad (A.8)$$

Equations (A.7) and (A.8) are then compared with Eqs. (A.2) and (A.3), respectively. Solving for a_2 with $\beta_1 = (a/b_2)^{1/N}$ in the first pair of equations and with $\beta_2 = (a/b_3)^{1/N}$ in the second pair of equations, we obtain two simultaneous equations involving a_2 and a_3 :

$$a_2 = (1+a_3)\beta_1^{2N/(N+1)} - 1 \quad (\text{A.9})$$

$$a_2 = (a_2+a_3)\beta_2^{2N/(N+1)} - 1 \quad (\text{A.10})$$

Equations (69) and (70) are obtained by solving Eqs. (A.9) and (A.10) for a_2 and a_3 in terms of β_1 and β_2 .

A.3 Uniaxial Tests at 45° on Y-Z , X-Y and Z-X Planes

Consider the case of the uniaxial test at 45° on the y-z plane. The stress applied at 45° to the coordinate axes in the plane is denoted by $\sigma_{45(yz)}$. The corresponding strain is denoted by $\epsilon_{45(yz)}$. By means of a stress transformation, the plane stress vector $[\sigma_{yy}, \sigma_{zz}, \sigma_{yz}]^T = [\sigma_{45(yz)}/2, \sigma_{45(yz)}/2, \sigma_{45(yz)}/2]^T$.

After computing the equivalent stress defined in Eq. (45), the inplane strains are computed using Eqs. (50)-(52):

$$\epsilon_{yy} = K a_1/6 \sigma_{45(yz)}^N \quad (\text{A.11})$$

$$\epsilon_{zz} = K a_3/6 \sigma_{45(yz)}^N \quad (\text{A.12})$$

$$\gamma_{yz} = K a_5 \sigma_{45(yz)}^N \quad (\text{A.13})$$

where

$$K = a \left(\frac{3}{a_1+a_2} \right)^{(N+1)/2} \left(\frac{a_1+a_3}{3} + 2a_5 \right)^{(N-1)/2} (1/2)^{(N-1)} \quad (\text{A.14})$$

The strain rate at 45° to the coordinate axis can be obtained by a strain transformation :

$$\epsilon_{45}(yz) = 1/4 \left(\frac{a_1 + a_3}{3} + 2a_5 \right) K \sigma_{45}(yz)^N \quad (A.15)$$

Comparison of Eqs. (A.4) and (A.15) with $\beta_3 = (a/b_4)^{1/N}$ yields an expression for a_5 , as given by Eq. (72). To obtain parameters a_4 and a_6 , (see Eqs. (71) and (73)), similar 45° tests can be conducted in the x-y and z-x planes respectively. For a transversely isotropic material, $\beta_2 = \beta_3 = 1$ and $\beta_4 = \beta_5$. The constants a_1 to a_5 can then be simplified to the following:

$$a_1 = 1 \quad (A.16)$$

$$a_2 = 2\beta_1^n - 1 \quad (A.17)$$

$$a_3 = 1 \quad (A.18)$$

$$a_4 = 2\beta_1^n / 6 (4\beta_4^{-n} - 1) \quad (A.19)$$

$$a_5 = 2\beta_1^n / 6 (4 - \beta_1^{-n}) \quad (A.20)$$

$$a_6 = 2\beta_1^n / 6 (4\beta_5^{-n} - 1) \quad (A.21)$$

APPENDIX B

Frederking's Tests

B.1 Type A Test

The coordinate axes are defined in the text. The ice sheet is subjected to normal stress σ_{yy} in the y-direction, and its in-plane movement in the z-direction is restrained. Stresses in the x-direction are assumed to be zero. Thus:

$$\sigma_{xx} = 0 \quad (B.1)$$

$$\epsilon_{zz} = 0 \quad (B.2)$$

The derivation below assumes that damage is negligible. Using Eqs. (50)-(52) and (B.2), the following expression is obtained:

$$\sigma_{zz} = \frac{a_2}{a_2 + a_3} \sigma_{yy} \quad (B.3)$$

After computing the equivalent stress (Eq. (45)), the strain rate in the y-direction is determined from Eqs. (50)-(52):

$$\dot{\epsilon}_{yy} = a \left[\frac{1}{1+a_2} \left(1 + \frac{a_2 a_3}{a_2 + a_3} \right) \right]^{(N+1)/2} (\sigma_{yy}^c)^N \quad (B.4)$$

where the superscript c on σ_{yy} implies that it is confined. For an unconfined test we have from Eq. (A.1):

$$\dot{\epsilon}_{yy} = a (\sigma_{yy}^u)^N \quad (B.5)$$

where the superscript u on σ_{yy} implies that it is unconfined. If the strain rates are the same, we can equate Eqs. (B.4) and (B.5) to obtain (with substitutions from Eqs. (A.16)-(A.21) for

transverse isotropy) the expression for Γ_z given by Eq. (74).

B.2 Type B Test

The load is applied in the y-direction. Stresses in the z-direction are assumed to be zero. Displacements are constrained in the x-direction. These imply:

$$\sigma_{zz} = 0 \quad (B.6)$$

$$\epsilon_{xx} = 0 \quad (B.7)$$

The same procedure is followed as in the type A test. The equations corresponding to Eqs. (B.3)-(B.4) are, respectively:

$$\sigma_{xx} = \frac{a_1}{a_1 + a_3} \sigma_{yy} \quad (B.8)$$

$$\epsilon_{yy} = a \left[\frac{1}{1 + a_2} \left(a_2 + \frac{a_3}{1 + a_3} \right) \right]^{(N+1)/2} (\sigma_{yy}^c)^N \quad (B.9)$$

Comparing Eqs. (B.9) and (B.5), and substituting from Eqs. (A.16)-(A.21), Eq. (75) for Γ_x follows.

APPENDIX C

Triaxial Test

In the triaxial test of a transversely isotropic ice sheet subjected to a normal stress σ in the y-direction, the stress state is described by the vector $[\sigma_{xx} \ \sigma_{yy} \ \sigma_{zz} \ \sigma_{xy} \ \sigma_{yz} \ \sigma_{zx}]^T = [\tau\sigma \ \sigma \ \tau\sigma \ 0 \ 0 \ 0]^T$, where τ is the ratio of the confining stress to the axial stress. The equivalent stress (Eq. (45)) is $\sigma_e = (1-\tau)\sigma$. The strain rate in the y-direction is obtained from Eqs. (50)-(52) as follows:

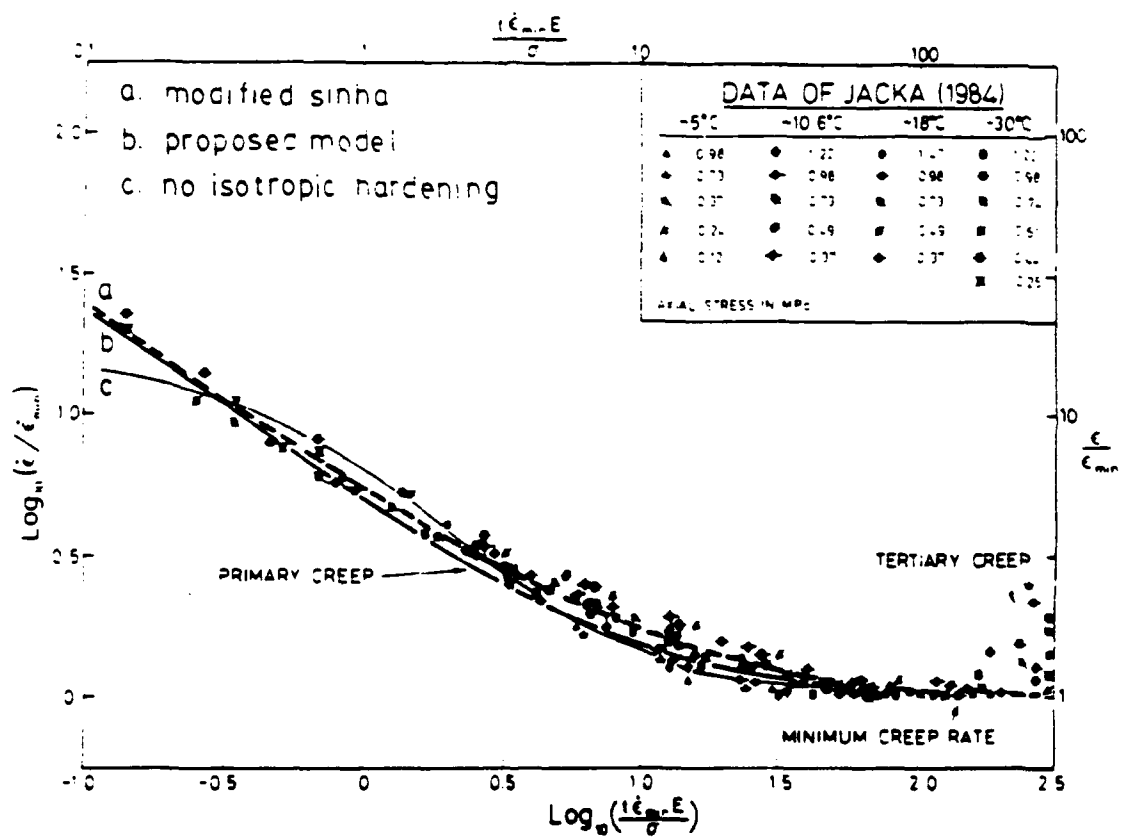
$$\dot{\epsilon}_{yy} = a(1-\tau)^N (\sigma_{yy}^{tr})^N \quad (C.1)$$

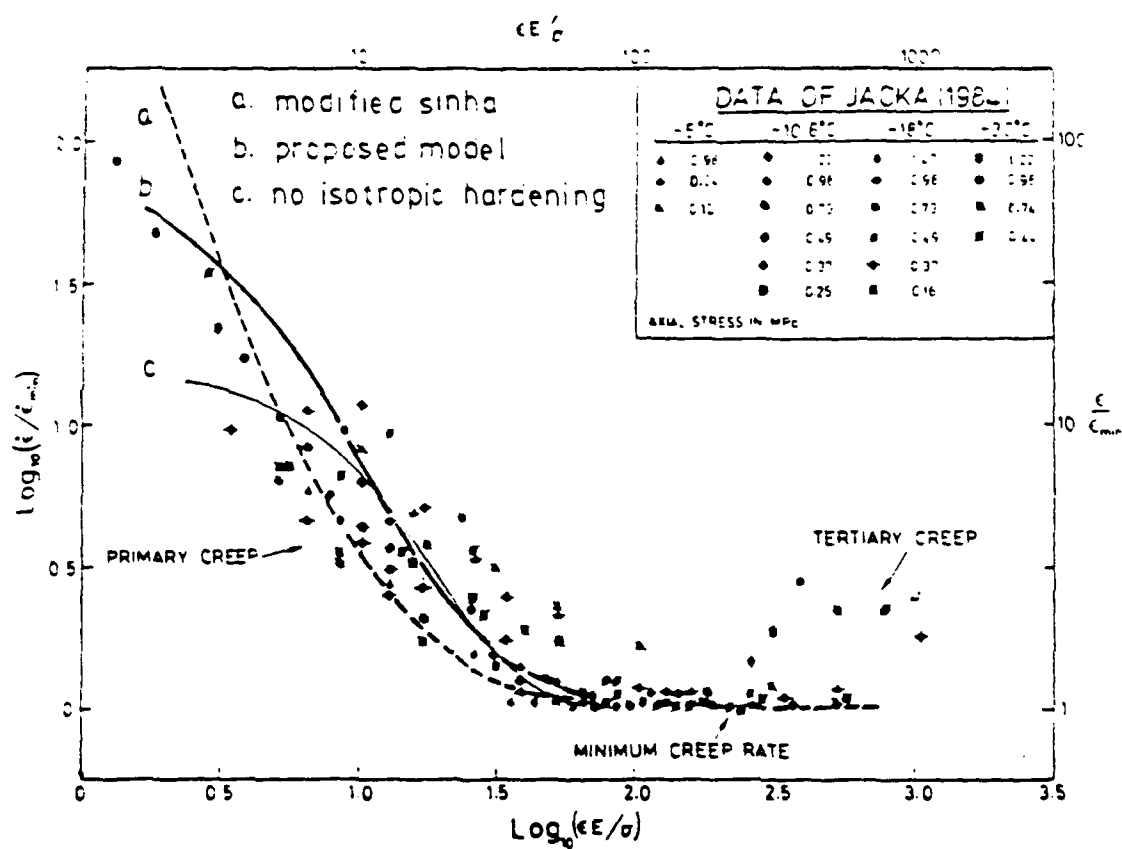
where the superscript 'tr' signifies loading under triaxial conditions. Combining Eqs. (B.5) and (C.1) yields Eq. (76). Also the shear stress normalized by the unconfined stress is independent of τ as shown below:

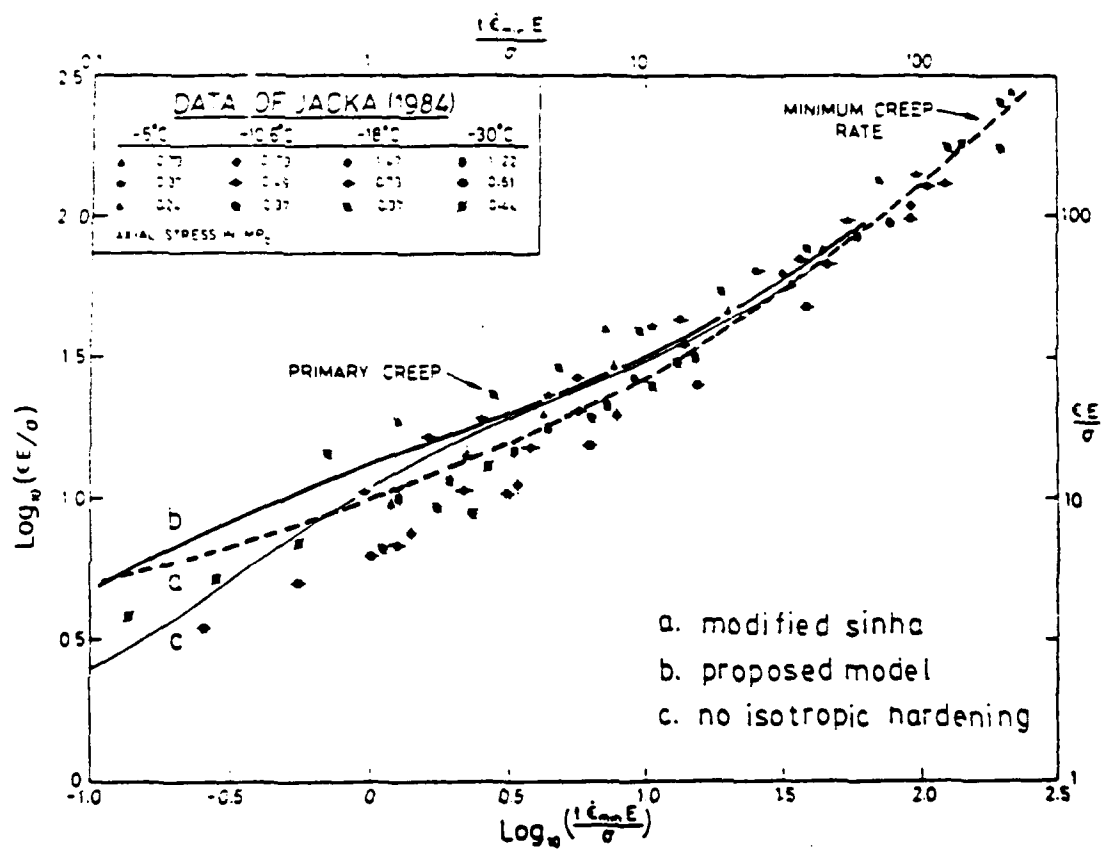
$$\frac{\sigma_{yy} - \sigma_{zz}}{\sigma_{yy}^u} = \frac{(1-\tau)\sigma_{yy}^{tr}}{\sigma_{yy}^u} = 1 \quad (C.2)$$

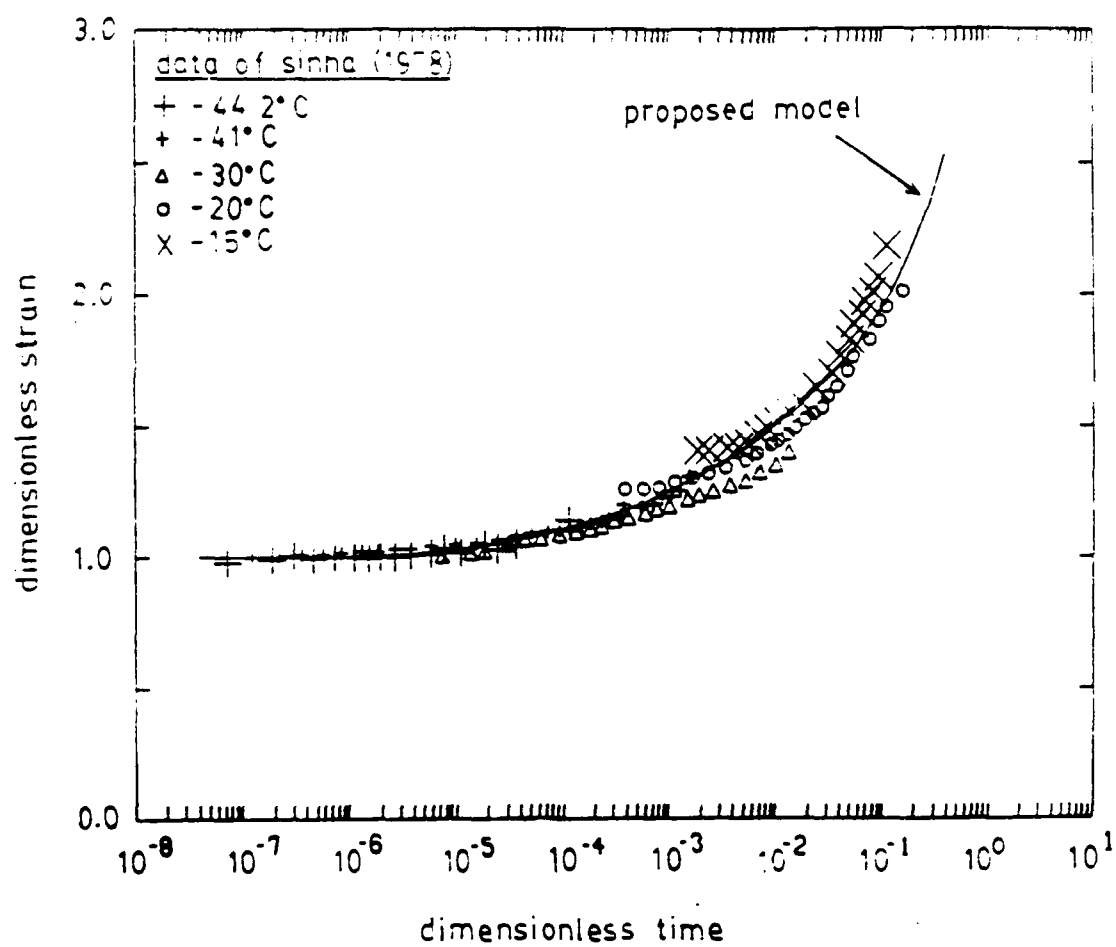
FIGURE CAPTIONS

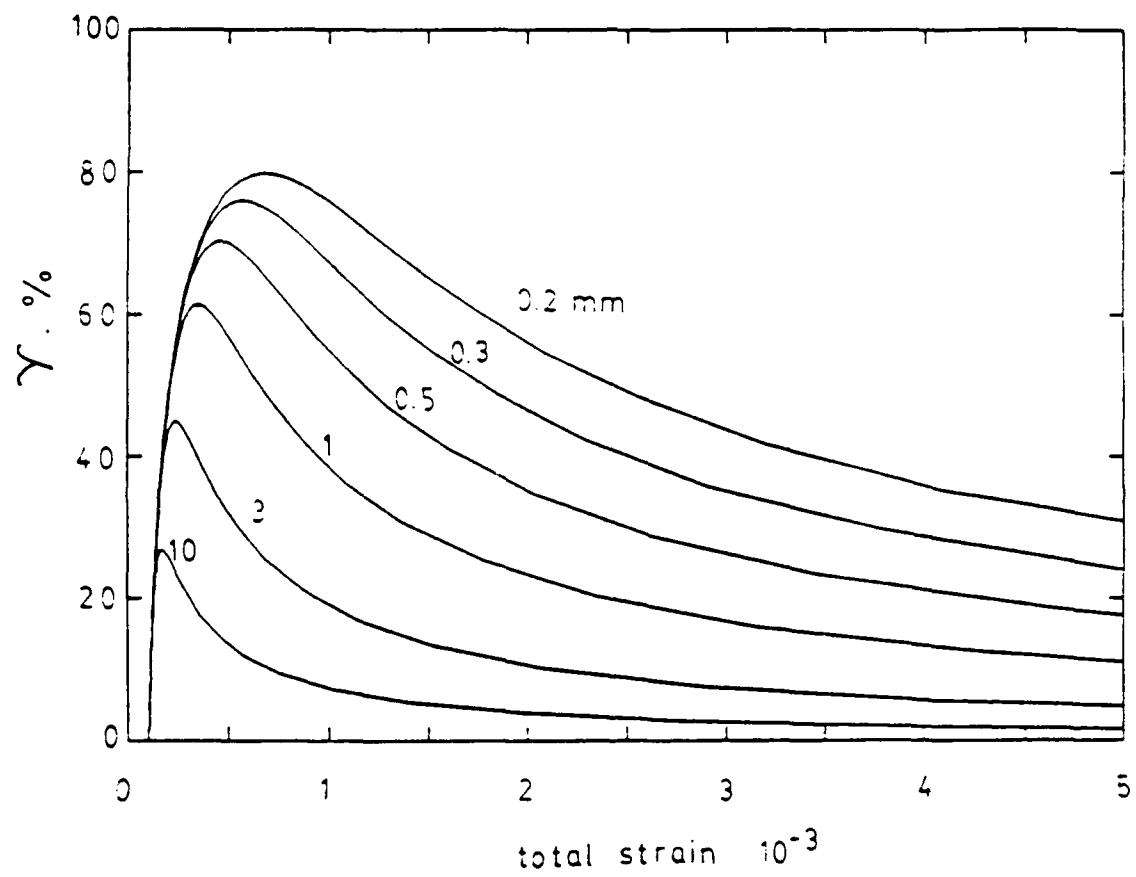
- Figure 1 Dimensionless Strain Rate Plotted Against Dimensionless Time, from the Data of Jacka (1984).
- Figure 2 Dimensionless Strain Rate Plotted Against Dimensionless Strain, from the Data of Jacka (1984).
- Figure 3 Dimensionless Strain Plotted Against Dimensionless Time, from the Data of Jacka (1984).
- Figure 4 Dimensionless Strain Plotted Against Dimensionless Time, from the Data of Sinha (1978).
- Figure 5 Strain Dependence of Ratio of Transient Strain to Total Strain for Various Grain Sizes; $\sigma=1.0$ MPa at -10°C .
- Figure 6 Stress and Strain History and Stress-Strain Results on Columnar-Grained Ice of Average Grain Diameter of 4.5 mm , at -10°C for Nominal Strain Rate of $5 \times 10^{-5}\text{ s}^{-1}$.
- Figure 7 Comparison Between the Predicted and Experimental Creep and Recovery of Snow Ice. Experimental Data of Brill and Camp Reproduced from Sinha (1979). The Zero Time of Curve (c) is Shifted for Clarity.

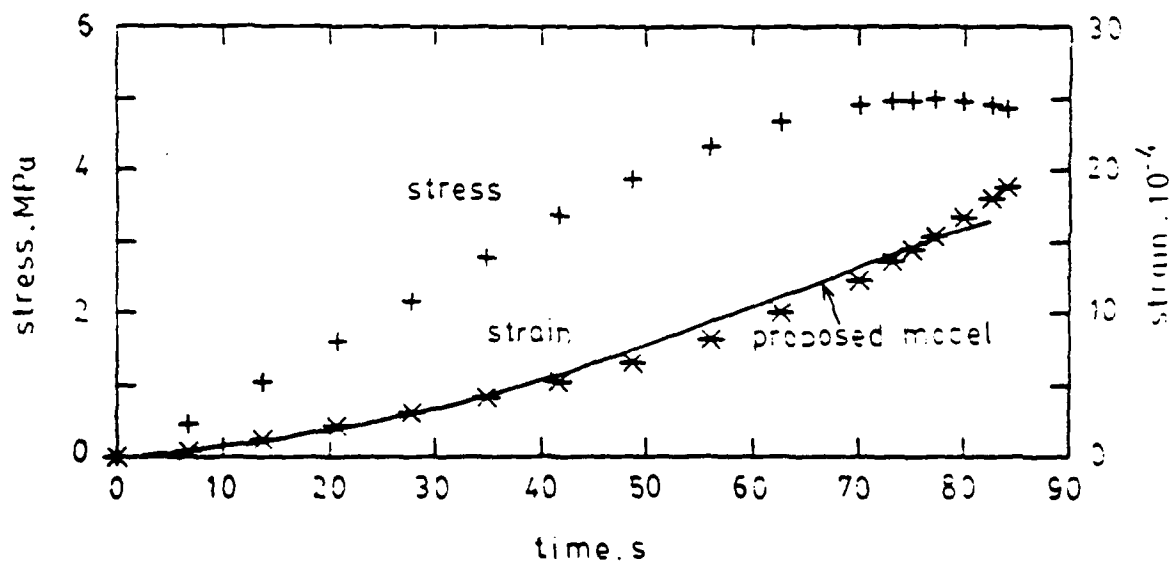
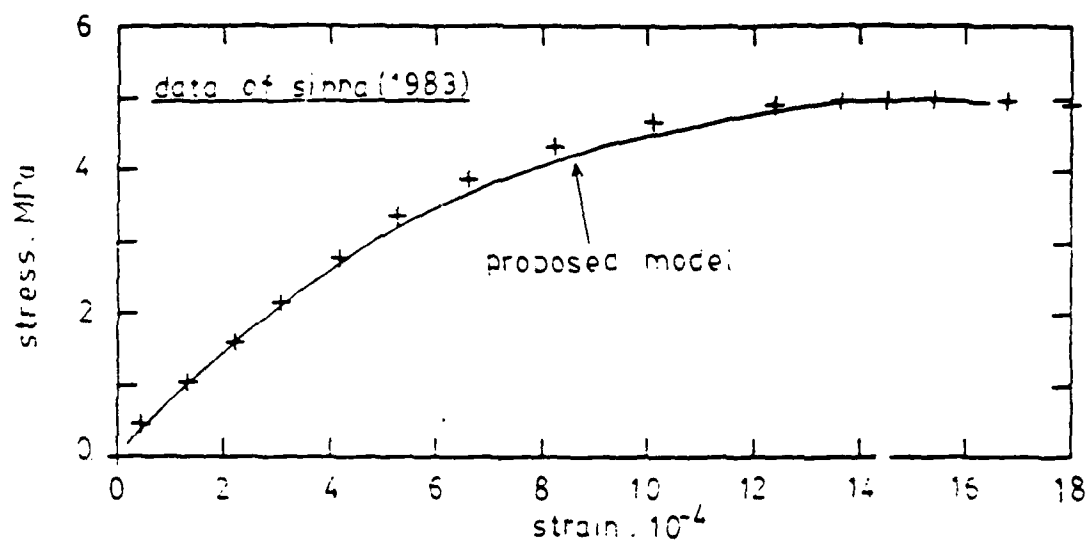


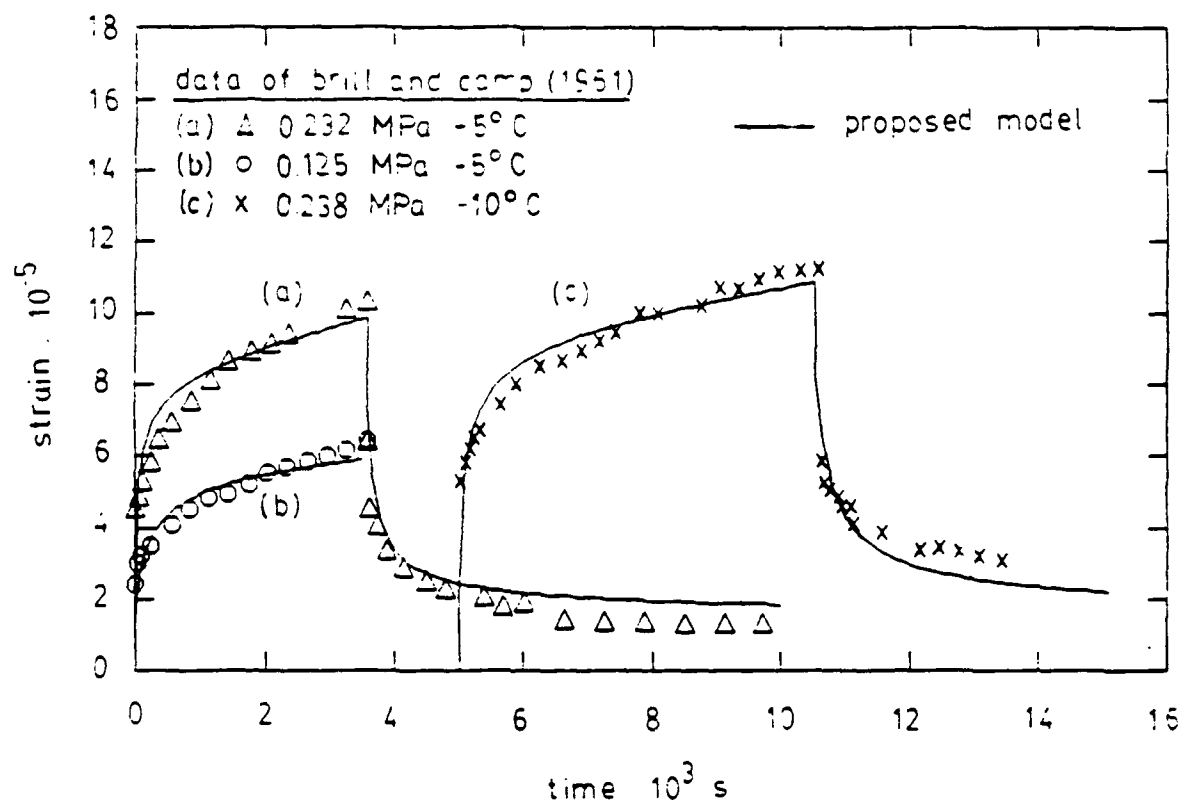












APPENDIX B

A RATE-SENSITIVE CONTINUUM DAMAGE MODEL FOR ICE

A RATE-SENSITIVE CONTINUUM DAMAGE MODEL FOR ICE

Mao S. Wu and S. Shyam Sunder

Massachusetts Institute of Technology, Department of Civil Engineering, Rm
1-274, Cambridge, MA 02139 (U.S.A.)

ABSTRACT

A rate-sensitive damage model is developed for describing the continuum behaviour of ice under variable loading conditions. The damage formulation employs a second rank symmetric tensor for describing the damage state of the material, a net stress tensor for specifying the evolution of damage, and an averaged net stress tensor for specifying the stress-strain laws. The rate of damage is assumed to depend on an isotropic component associated with the distortional stress and an anisotropic component associated with the maximum principal deviatoric stress. Pressure melting is accounted for by means of a relation between the creep resistance parameter in Glen's power law and temperature corrected for the effect of hydrostatic stress. Integrated with the generalized Maxwell formulation and assuming an initially isotropic material, the model can (a) describe anisotropic damage behaviour under multiaxial and non-steady states of stress, (b) capture the pressure sensitivity of ice, and (c) model pressure melting of ice under large hydrostatic stresses. Verification of the model is achieved with several independent sets of data, including those for first-year sea ice and freshwater ice.

1. INTRODUCTION

The theory of plasticity has been successfully applied to ductile materials, but is generally unsuitable for describing the behaviour of brittle materials. This is because it was originally developed as a phenomenological theory for modelling nonlinear behaviour due to such irreversible microstructural changes as crystalline slip and twinning, whereas the nonline-

arity of brittle materials is primarily due to the nucleation and growth of microcracks. It is this inherent deficiency in the theory of plasticity that has encouraged the application of damage mechanics in formulating the constitutive laws for a general material in which several distinctly different mechanisms, including microcracking and rate-independent (or dependent) viscoelastic processes, may occur simultaneously.

The concept of damage as an internal variable which reflects the accumulation of internal defects was pioneered by Kachanov (1958), who used the complementary idea of 'continuity' as a variable for modelling brittle creep rupture of materials. Since then, damage mechanics has been used for modelling the behaviour of brittle rock (Kachanov, 1982; Costin, 1983, 1985a,b), concrete (Fonseka and Krajcinovic, 1981; Ortiz, 1985; Wu, 1985), and of course metals (Leckie and Hayhurst, 1974; Murakami and Ohno, 1978; Chaboche, 1981, 1984; Levy, 1985).

Ice under compressive loading behaves as a continuum undergoing damage, which is particularly significant in the ductile to brittle transition region. Indeed, damage leads to strain softening under constant strainrate loading, and to tertiary creep under constant stress loading. Moreover, unloading a damaged material often shows a reduction in the elastic modulus. These observations have stimulated the application of damage concepts in the constitutive modelling of ice (Karr, 1985; Szyszkowski and Glockner, 1986). However, the former model is limited to one-dimensional applications, and both models assume that damage can be described by a scalar variable, i.e., the anisotropic nature of damage is ignored. This is in contradiction to microstructural observations of many materials which show that creep defects can be orientated on planes perpendicular to the maximum principal tensile stress. Such anisotropy is especially important under non-proportional loading

when conditions for rupture or failure often vary according to the particular loading history of the material.

Damage in ice is also known to be sensitive to strainrate, i.e., the evolution of damage is closely related to the development of creep strain. This is because in the creep damage process the nucleation and growth of microcavities can be influenced by diffusion, by dislocation creep, and by stress concentration at irregularities on the grain boundary caused by grain boundary sliding (Sinha, 1984). All these processes are linked to the development of creep strain, which therefore affects damage growth.

Ice is also a pressure sensitive material, particularly under high strainrate loading, which means it has a higher shear strength under confinement than under uniaxial compression. This is due to the suppression of microcracking by the confining stress. For very low strainrate loading, microcracking is not significant and little or no pressure sensitivity is observed. On the other hand, it is known that the shear resistance of ice decreases under large confining stress, and ultimately vanishes at the pressure corresponding to phase change. This mode of microstructural change, together with the phenomenon of pressure sensitivity discussed above, have been considered indirectly through the formulation of three-dimensional yield envelopes based on experimental data of conventional triaxial tests (Nadreau, 1986).

The present study develops a more elaborate continuum damage theory for the model proposed by Ting and Shyam Sunder (1985, 1986). It integrates an anisotropic damage theory and a pressure melting model with the generalized Maxwell formulation adopted in the original model. Based on the assumption of an initially isotropic material, the current model can (a) describe anisotropic damage behaviour under complex stress fields, (b) capture the pressure

sensitivity characteristic of ice, and (c) model the pressure melting behaviour of ice under large hydrostatic stresses. Verification of the model is achieved with several independent sets of data, including those for first year sea ice and freshwater ice.

2. CONTINUUM DAMAGE MODELLING OF ICE

The formulation of continuum damage models typically consists of three critical steps. These are (a) the selection of a damage variable based on an appropriate averaging over a representative volume, (b) the establishment of the damage evolution laws, and (c) the adoption of a set of constitutive relations. Intense debate exists as to how a damage model should be constructed. Krajcinovic (1983a, b, 1985a, b, c) firmly supported the use of a vectorial damage variable to describe a field of flat, planar microcracks, while the traditional predilection for second rank tensors has led to such representation of the damage state by Kachanov (1980), Murakami and Ohno (1981), and many others. The formulation of the damage evolution equations can be accomplished by either prescribing an independent law for each component of the damage tensor (Chaboche, 1981; Murakami and Ohno, 1981; Costin, 1985a, b) or by using the concept of a damage surface (Dragon and Mroz, 1979; Krajcinovic and Fonseka, 1981). Lack of space precludes a detailed review of these various approaches; for critical appraisal see Krajcinovic (1985a, b) and Kachanov (1985). We shall discuss only the damage theory of Murakami and Ohno (1981) upon which the damage formulation is based.

Damage Tensor :- In this theory, the microcracks are directly used to define the damage variable tensor through the reduction in the strength of sections. For an elementary volume V of the damaged material continuum containing n microcracks, it was shown that the damage state can be defined

by the following second rank symmetric tensor \underline{D} :

$$\underline{D} = \frac{1}{S(V)/3} \sum_{k=1}^n \int_V \underline{N}_k \times \underline{N}_k dS_k \quad (1)$$

where dS_k is the area of the k -th microcrack, \underline{N}_k the unit vector normal to dS_k , and $S(V)$ the total area of grain boundaries in V . The symbol \times denotes tensor product of two vectors, the resulting quantity being a second rank tensor. \underline{D} can be rewritten in terms of its principal values D_j and corresponding principal directions \underline{N}_j ($j = 1, 2, 3$) so that

$$\underline{D} = \sum_{j=1}^3 D_j \underline{N}_j \times \underline{N}_j \quad (2)$$

where D_j represents the surface density of the microcracks in the principal plane perpendicular to \underline{N}_j (Fig. 1a). The damage effects on an arbitrary plane can be examined by means of the Cauchy tetrahedron OABC (Fig. 1b). It shows that due to damage on the three principal planes, the plane ABC, defined by the undamaged area vector $S\underline{v}$ where S is the area of and \underline{v} the unit normal to the surface, can be visualized as transforming into the fictitious plane A'B'C' described by the net area vector $S'\underline{v}'$. It can be shown that the two area vectors are related through the tensor $(\underline{1} - \underline{D})$:

$$S'\underline{v}' = (\underline{1} - \underline{D})S\underline{v} \quad (3)$$

The damage representation described above means that (a) an arbitrary damage

field can be described in terms of three mutually orthogonal systems of parallel microcracks, (b) the effect of a multitude of damage fields is in general obtained by summing the different damage tensors (one for each field), (c) the effect of damage in a plane of arbitrary orientation is to transform it into a plane of diminished area and different orientation, and (d) the tensor $(1 - \underline{D})$ in Eq.(3) can be interpreted as a linear transformation between the area vector \underline{Sv} and the net area vector $\underline{S'v'}$.

Damage Effect Tensor and Net Stress Tensor :-The reduction in area of a plane magnifies the stress tensor. If $\underline{\sigma}$ denotes the Cauchy stress acting on the tetrahedron OABC (Fig.1b), then the force vector acting on the surface \underline{Sv} is obtained using Cauchy's formula

$$\underline{St} = \underline{\sigma}(\underline{Sv}) \quad (4)$$

where \underline{t} is the corresponding stress vector. The effective surface element $\underline{S'v'}$ is subjected to the same force vector. Equating the two force vectors results in

$$\underline{\sigma}'(\underline{S'v'}) = \underline{\sigma}(\underline{Sv}) \quad (5)$$

which upon substitution from Eq.(3) gives

$$\underline{\sigma}'(\underline{S'v'}) = \underline{\sigma}(1 - \underline{D})^{-1}(\underline{S'v'}) \quad (6)$$

In Eq. (5) above, $\underline{\sigma}'$ is the net stress tensor and its relationship with the

Cauchy stress is evident from Eq. (6), i.e.

$$\underline{\sigma}' = \underline{\sigma}(\underline{1} - \underline{D})^{-1} \quad (7)$$

The net stress $\underline{\sigma}'$ is not necessarily symmetric; for the purpose of computation we use only its symmetric part

$$\underline{\sigma}' = \frac{1}{2} (\underline{\sigma} \underline{\phi} + \underline{\phi} \underline{\sigma}) \quad (8)$$

where

$$\underline{\phi} = (\underline{1} - \underline{D})^{-1} \quad (9)$$

The tensor $\underline{\phi}$ expresses the effect of damage on the Cauchy stress and is termed the damage effect tensor. It can also be thought of as a quantity which represents the effect of local stress concentration which influences the growth of damage. Physically, the above formulation implies that the effect of the Cauchy stress acting on a volume element OABC of a damaged continuum is identical to that of the net stress acting on the corresponding fictitious element O'A'B'C' without damage. The net stress is thus the locally magnified stress which governs the evolution of damage, i.e., the damage growth laws are specified with respect to the net stress tensor. Eq. (7) or Eq. (8) is the three-dimensional generalization of the net stress employed in the classical damage theory of Kachanov and Rabotnov.

Net Stress Tensor for Constitutive Relations :- In Eq. (8) it is seen that the transformation between the Cauchy stress tensor and the net stress tensor is specified by the second rank damage effect tensor, although a

transformation between two second rank tensors should be specified by a fourth rank tensor. The result of this transformation is that of the two subscripts of the Cauchy stress tensor, only one is transformed. The implicit assumption is that creep damage affects the stress only through the change of the effective area on which stress acts, and not through their three-dimensional arrangement. While this is generally true for damage growth, the deformation characteristics of damaged materials may depend on both area reduction and the three-dimensional arrangement of the microdefects. The net stress tensor described above therefore strictly cannot be used to specify the constitutive relations.

Murakami and co-workers (1982, 1983, 1986) proposed the use of a fourth rank net stress tensor constructed from a rather complex fourth rank damage effect tensor. However, by measuring the uniaxial tensile stress of brass specimens perforated with holes at different angles, they found that if the cavity density was below a certain limit, the uniaxial tensile stress was essentially the same regardless of the orientations of the perforations, and that this limit usually exceeds that corresponding to rupture of the material. This implies that the effect of material damage on creep deformation may be isotropic when the cavity density is less than a critical limit, and this may be valid just before failure. In view of these experimental observations, it was proposed that the net stress tensor for constitutive relations (averaged net stress tensor) may be defined through a scalar invariant of the damage effect tensor as follows

$$\underline{\underline{\sigma}}_n = (n + (1 - n)/3 \text{ tr } \underline{\underline{\epsilon}}) \underline{\underline{\epsilon}} \quad 0 < n < 1 \quad (10)$$

where n is a material constant.

Evolution Equations of Damage: -It must be stated at the outset that it is the net stress that is used in the damage laws. To avoid cumbersome terminology, however, we shall drop the word 'net' in the description of the stresses. For the proposed model, it is postulated that the rate of damage growth is governed by the local state of stress $\underline{\sigma}'$, the effect of the local stress concentration at the microcavities expressed through the damage effect tensor $\underline{\phi}$, the effective total strainrate $\dot{\epsilon}_e$ and the temperature T , i.e.,

$$\dot{\underline{D}} = \underline{F}(\underline{\sigma}', \underline{\phi}, \dot{\epsilon}_e, T) \quad (11)$$

To obtain Eq. (11) in explicit form, we can make use of tensor function theory as well as experimental observations. For many materials microcracks may form in planes perpendicular to the principal tensile stress, and may also develop isotropically. Under a non-hydrostatic compressive state of stress, local tensile fields can arise from material property mismatch between grains or from contact stresses between grains with irregular grain boundaries (Costin, 1983). These local tensile stresses will result in the nucleation and growth of microcracks. Since the normals to these microcracks are usually orientated in the directions of the principal tensile deviatoric stresses, it can be assumed that the local tensile stresses are proportional in magnitude to the principal tensile deviatoric stresses (henceforth principal deviatoric stresses) and also act in the same directions. Thus, damage may be assumed to develop in the directions \underline{v}_i and \underline{v}_{-i} ($i = 1, 2, 3$) of the positive (tensile) principal values of $\underline{\sigma}'$ and its deviator \underline{S}' , as well as isotropically in all three principal directions. For this model, we further postulate that damage develops in the direction of the maximum principal deviatoric stress since it

is predominantly in this direction that microcracks evolve under axial compression. This is referred to as the principal stress damage law (Murakami and Ohno, 1978).

For many brittle materials, the volumetric or bulk stress is known to suppress the formation and growth of microcracks. This phenomenon is also true for ice, especially at high rates of loading (Mellor, 1983), and can be modelled by mitigating the damage due to the maximum principal deviatoric stress. The amount of damage that is suppressed depends on the magnitude of the volumetric stress. For very large volumetric stress, the damage due to the maximum principal deviatoric stress may be completely suppressed. Seen from a different angle, the above formulation is equivalent to a decoupling of the applied stresses into deviatoric and volumetric components with different weighting factors.

It is conceivable that material damage can also be attributed to the distortional stress, or the effective stress. This isotropic damage is related to the second invariant of the deviatoric stress tensor, and the damage evolution is termed the J_2 damage law (Murakami and Ohno, 1978). The volumetric stress suppresses the microcracks and leads to increase in material strength and hence the distortional stress. The large distortional stress will induce damage and consequently limits the gain in strength due to the increase in volumetric stress. Note that the J_2 damage law may become dominant under moderate and large confining stresses when anisotropic damage is significantly suppressed.

The above reasoning implies that the damage evolution laws consist of two parts -an anisotropic part due to the maximum principal deviatoric stress, appropriately reduced according to the magnitude of the hydrostatic stress, and an isotropic part due to the effective stress.

To incorporate the effect of strainrate on damage, it is proposed that a power law holds between the damage growth rate and the effective total strainrate, i.e.,

$$\dot{D} \propto (\dot{\epsilon}_e)^{C_1} \quad (12)$$

The effect of the local stress concentration on damage evolution can be taken into account by incorporating invariants of the damage effect tensor in the damage evolution equations. For the isotropic part, the invariant $(1/3 \text{tr} \underline{e}^2)^{1/2}$, which is related to the root mean square of the diagonal terms of the damage effect tensor, is adopted. For the anisotropic part, the invariant $\text{tr}(\underline{e} \underline{v}_D^1 \otimes \underline{v}_D^1)$ is used, where \underline{v}_D^1 denotes the direction cosine vector of the maximum principal deviatoric stress. This expression simply evaluates the magnitude of the damage effect tensor in the direction of the maximum principal deviatoric stress. Thus, for the case of plane stress, $\underline{v}_D^1 = (\cos \theta^1, \sin \theta^1)$, where θ^1 is the angle between the maximum principal deviatoric stress and the reference x-axis, and $\text{tr}(\underline{e} \underline{v}_D^1 \otimes \underline{v}_D^1)$ is the familiar expression $\phi_{11} \cos^2 \theta^1 + 2\phi_{12} \cos \theta^1 \sin \theta^1 + \phi_{22} \sin^2 \theta^1$.

The principal damage axes \underline{v}_D^1 , \underline{v}_D^2 and \underline{v}_D^3 in general do not remain fixed with respect to the reference axes x_1 , x_2 and x_3 , especially for the case of a non-steady state of stress in which the maximum principal deviatoric stress may rotate in an arbitrary fashion with time. The relative amount of damage in the x_1 , x_2 , x_3 , x_1 - x_2 , x_2 - x_3 and x_3 - x_1 directions at any instant of time is determined by the tensor product $\underline{v}_D^1 \otimes \underline{v}_D^1$. For plane stress the relative amount of damage is $\cos^2 \theta^1$ in the x_1 direction, $\sin^2 \theta^1$ in the x_2 direction, and $\sin \theta^1 \cos \theta^1$ in the x_1 - x_2 direction. If there are two equal

principal stresses, as in the case of conventional triaxial loading, we have to sum the contributions from each principal stress.

The proposed damage evolution equations are based on the concepts discussed above. They can be written in the following form :

$$\dot{\underline{D}} = \dot{\underline{D}}_A + \dot{\underline{D}}_I \quad (13)$$

where A and I denote 'anisotropic' and 'isotropic' respectively, and

$$\dot{\underline{D}}_A = \dot{\epsilon}_e^{c_1} (\text{tr} \underline{\underline{v}}_D^1 \times \underline{\underline{v}}_D^1)^{c_2} \langle \alpha S^1 + \beta I_1'/3 \rangle^N \underline{\underline{v}}_D^1 \times \underline{\underline{v}}_D^1 \quad (14)$$

$$\dot{\underline{D}}_I = \dot{\epsilon}_e^{c_1} (1/3 \text{tr} \underline{\underline{e}}^2)^{c_2/2} (\gamma (3J_2')^{1/2})^N \underline{\underline{1}} \quad (15)$$

In Eqs.(14) and (15), c_1 , c_2 , α , β and γ are material constants. N is the power law index for ice; here we have assumed that the same power governs the deformation characteristics as well as the damage behaviour. S^1 , $I_1'/3$ and $(3J_2')^{1/2}$ denote the maximum principal deviatoric stress, the volumetric stress and the effective stress, respectively. The dash sign indicates net stress, i.e.,

$$S^1 = \max(S_i'), \quad i = 1, 2, 3 \quad (16)$$

$$I_1' = I_1(\sigma') \quad (17)$$

$$J_2' = J_2(\sigma') \quad (18)$$

and the quantity inside the angle brackets, if negative, is assigned a value of zero. Other symbols are as defined previously.

Constitutive Relations: -The constitutive laws for the proposed model are based on the generalized Maxwell formulation adopted in the original model of Ting and Shyam Sunder (1985). These laws are reproduced below for the isotropic case; they are merely a special case of the original model with the orthotropic parameters a_1 to a_6 equal to 1. It must be emphasized that 'stress' in this section actually refers to the 'averaged net stress' defined by Eq. (10).

The total strainrate tensor $\dot{\underline{\epsilon}}$ can be decomposed into the elastic strainrate tensor $\underline{C} \dot{\underline{\epsilon}}$ and the creep strainrate tensor $\dot{\underline{\epsilon}}_{cr}$. The latter can be further decoupled into the delayed elastic tensor and the secondary creep strainrate tensor. Damage is incorporated through the averaged net stress tensor, and affects all the strain components identified above, thus resulting in tertiary creep. The governing equations, in engineering notation of stresses and strains, are :

$$\dot{\underline{\epsilon}} = \underline{C} \dot{\underline{\epsilon}}_a + \dot{\underline{\epsilon}}_{cr} \quad (19)$$

$$\dot{\underline{\epsilon}}_{cr} = \lambda_a \underline{S}_a \quad (20)$$

where

$$\lambda_a = \frac{3}{2} \frac{1}{c_{ae}} \left(\frac{\dot{\underline{\epsilon}}_a e}{E_d} + \left(\frac{M}{A} \sigma_{ae} \right)^N \right) \quad (21)$$

In Eq. (20), \underline{S}_a is the conventional deviatoric stress tensor. c_{ae} in Eq. (21) is the effective stress for isotropic materials. The two terms in Eq. (21) are associated with the delayed elastic component and the secondary creep strain component, the latter being the multiaxial form of Glen's power law. M and A

are creep resistance parameters. E_d is the modulus of elasticity given by

$$E_d = E(1/r \exp(A/E \dot{\epsilon}_e^{1/N}) - 1) \quad (22)$$

where E is Young's modulus and r a constant.

Pending experimental verification, we assume in this model that the averaged net stress is given by Eq. (10) with $\eta = 0$, that is,

$$\underline{\sigma}_a = (1/3 \operatorname{tr} \underline{\sigma}) \underline{\sigma} \quad (23)$$

This implies that the net stress affecting the global stress-strain behaviour is governed only by the average damage effect on stress.

3. PRESSURE MELTING MODEL

Ice is known to change into liquid form at a certain level of hydrostatic pressure. Triaxial testing of ice was carried out only relatively recently (Jones, 1978, 1982 ; Hausler, 1981; Richter-Menge et al. , 1985; Nadreau, 1986), but analyses have already been done on the available data to determine a three-dimensional yield envelope for ice. Unfortunately, most of these analyses do not take into account the decreasing resistance of ice as the hydrostatic pressure increases.

Nadreau (1986) proposed a new yield envelope which was calibrated with his own test data and also results performed on freshwater ice from Jones. This three-dimensional envelope is teardrop-shaped and for isotropic ice is symmetrical about the hydrostatic axis. The size of this envelope increases as the strainrate increases. Indeed, according to Mellor (1983), for very small

strainrates the deviatoric yield stress decreases steadily as the hydrostatic stress increases until it vanishes at the pressure corresponding to phase change. The yield envelope is a cone symmetrical about the hydrostatic axis. For high strainrates, the deviatoric yield stress increases initially, but eventually decreases as the hydrostatic stress becomes sufficiently large. The yield envelope is thus similar to the teardrop surface proposed by Nadreau.

The current model will predict increasing deviatoric yield stress with increasing hydrostatic stress. It will also predict a peak with subsequent reduction in the deviatoric yield stress. This occurs when the hydrostatic stress is large enough so that any suppression of damage is offset by the increase in damage due to the large distortional stress. At large hydrostatic stress, however, the phenomenon of pressure melting becomes important. In order to incorporate this effect, it is proposed that the creep resistance parameter A in Eq. (21) decreases with increasing hydrostatic stress. The pressure melting model will be briefly discussed in the following paragraphs.

The value of the creep resistance parameter A at any temperature T and hydrostatic pressure p is obtained through a temperature correction, that is, is equal to the value at an equivalent temperature T' and zero hydrostatic pressure. Mathematically, this is expressed as

$$A(T, p) = A(T', 0) \quad (24)$$

where the equivalent temperature is defined as

$$T' = T + (T_0 - T_m) \quad (25)$$

In Eq. (25), T_0 is the melting temperature at zero hydrostatic pressure, and

T_m is the melting temperature at some hydrostatic pressure p . The value of T_m can be obtained from the phase diagram shown in Fig.2 (from Nadreau, 1986), or from the following relation proposed for ice 1h, valid between $T_0 = 273$ K for pure ice (or 271 K for sea ice) and some reference temperature T_1 (e.g. 251 K), and between 0 MPa and some reference hydrostatic pressure p_1 (e.g. 200 MPa) :

$$T_m(p) = T_1 + (T_0 - T_1) (1 - (p/p_1)^\xi)^{1/\xi} \quad (26)$$

where ξ is a constant which describes the curvature of the temperature versus pressure curve. Typically, ξ varies between 1 and 1.2; for the former value, the curve is linear. An average value of 1.05 is used in this study. Also, the trend of experimental data (Richter-Menge et al., 1985) suggests that an appropriate value for p_1 to be 50 MPa for sea ice.

Having obtained the value of the equivalent temperature using Eqs.(26) and (25), we can determine the value of $\dot{\epsilon}$ according to the following relations :

$$\dot{\epsilon} = A_0 \exp[-Q/(NRT')] \quad T' < 263 \text{ K} \quad (27)$$

$$\dot{\epsilon}/A(263, 0) = [(T_0 - T')/(T_0 - 263)]^\zeta \quad T' > 263 \text{ K} \quad (28)$$

where $A(263, 0)$ is the creep resistance at $T = 263$ K (and $p = 0$ MPa) and ζ is a constant determined by the requirement of continuity in the slope between the two curves at $T = 263$ K (see Fig. 3). ζ is equal to 0.377 for pure ice and equal to 0.301 for sea ice for this formulation. Q , N and R are the activation energy, the power law index for ice and the universal gas constant respectively. A_0 is a temperature independent constant.

4. EXPERIMENTAL VERIFICATION

The model is verified against several independent sets of experimental data obtained from constant strainrate tests. The following values for the model parameters provide an average representation of the data:

E = 9500 MPa
r = 0.65
A₀ = 9.2 MPa s^{1/N}
N = 3
M = 1411
Q = 65000 J mol⁻¹

The universal gas constant is equal to 8.314 J mol⁻¹ K⁻¹. The damage model introduces five material dependent parameters α , β , γ , c_1 and c_2 to model anisotropic/isotropic damage, pressure sensitivity, strainrate sensitivity and the effect of local stress concentration on damage. More precisely, α , β and γ are associated with the maximum principal deviatoric stress, the volumetric stress and the effective stress, respectively. c_1 is a constant which determines the rate of damage due to the strainrate effect while c_2 is associated with the contribution to damage growth due to the damage effect or the effect of local stress concentration.

Typically, α lies between 1 and 70, β between 0 and 20, and γ between 0 and 1. Their units are given by MPa⁻¹ s^{(c₁-1)/N}. Note the rather wide range of values α can assume: a large α will result in the lowering of the maximum stress versus strainrate curve in the ductile to brittle transition region (case 1), while a smaller α will cause departure from the power law model prediction, although not necessarily result in a lowering of the above-mentioned curve (case 2). α also determines the magnitude of the peak stress. The ratio α/β is usually greater than about 2. γ is usually small compared to α , reflecting the fact that damage evolution is generally governed by the principal stress law rather than the J_2 law. However, the J_2 law can be

important under large hydrostatic stresses when the damage due to the maximum principal stress is significantly suppressed. This suggests that the material deforms in a pseudo-ductile manner with large scale deformation being taken up by many homogeneously distributed cracks, as is the case for brittle solids with microcracks or pores under large compressive stress states (Ashby and Hallam, 1986). c_1 typically lies between 0.2 and 2.5, while c_2 can assume any value between 0 and 2. The smaller the value of c_1 , the greater will be the damage rate. If c_2 is large, very severe post-peak strain softening under constant strainrate loading can be expected. Table 1 gives the values of the five parameters which provide an average representation of available experimental data corresponding to zero salinity and $T = -10^\circ\text{C}$ for the two cases mentioned above.

Fig. 4 shows the maximum stress or strength observed from constant strainrate tests on columnar pure and sea ice versus strainrate (case 1). The experimental data has been normalized for the temperature of -10°C and zero salinity. The solid line in the figure represents the prediction of the current model using the first set of damage parameters in Table 1; it is seen that the model captures the overall trend of the data very well, particularly the severe strain-softening behaviour in the ductile to brittle transition region. For strainrates greater than 10^{-2} s^{-1} the continuum model is invalid and a horizontal line representing sudden failure by brittle fracture is drawn at the stress level of 5 MPa. The dashed line indicates the prediction of the power law model which does not consider in its formulation the concept of damage. The effect of temperature on the strength versus strainrate behaviour is shown in Fig. 5, which shows that with decreasing temperature the maximum strength increases and also occurs at lower strainrates. At the strainrates of 10^{-3} and 10^{-6} s^{-1} , the strength at -40°C is about twice and quadruple that

at -10°C , respectively. The same plot also suggests that in the region dominated by brittle behaviour, the strength becomes insensitive to temperature. These predictions agree well with Mellor's observations (see Fig. 35 of Mellor, 1983). The evolution of damage parallel to the compressive axis with respect to strains and strainrates is illustrated in Fig. 6. It is observed that damage is insignificant at very small strains and strainrates, and eventually levels off. The latter observation implies that the evolution of axial damage under compression is relatively stable compared to the tensile fracture of a brittle solid (Ashby and Hallam, 1986; Nemat-Nasser and Horii, 1982).

Some researchers (e.g. Mellor, 1983) have suggested that the maximum stress versus strainrate behaviour deviates from the power law predictions but does not exhibit a peak with subsequent reduction, as illustrated in Fig. 7. This corresponds to case (2) in the present study. The model predictions using the second set of damage parameters in Table 1 and $N = 2.5$ are superimposed on the experimental data. The motivation for using a smaller N in this single instance is to match the slope of the curve at very small strainrates, but this also requires the use of a larger A , equal to $650000 \text{ MPa s}^{1/N}$. It is seen that the model can capture the characteristics displayed by Gold's data for various ice types corresponding to the temperature of -10°C and density of 0.9 Mg/m^3 .

The proposed model has also been verified against the triaxial test results of Richter-Menge et al. (1985), Jones (1982) and Nadreau (1986).

In the tests performed by the former, the columnar first-year sea ice samples were horizontally cored in three directions and at different depths of the ice block. The direction of testing is specified by the angle between the compressive axis and the c-axis of the ice ($\sigma : c$). The confining pressure is

ramped in fixed proportion to the applied stress in the uniaxial direction. The four ratios of confining pressure to axial pressure used in their tests are $\tau = 0, 0.25, 0.5$ and 0.75 .

The model predictions of the stress-strain behaviour for $\sigma : c = 0^\circ$ and for the two strainrates of 10^{-3} and 10^{-5} s^{-1} are shown in Fig. 8. The same figure also plots the experimental data, suitably averaged through the thickness of the ice block. Note the suppression of damage reflected through the decrease in strain-softening in the stress-strain behaviour as the confining pressure increases. The corresponding normalized shear strength versus confining pressure curves are plotted in Fig. 9. It is observed that the pressure sensitivity of sea ice is moderate, with only about 25% increase in shear strength. As τ equals 0.75 , pressure melting has become dominant. It can be concluded that the model gives reasonably good predictions of the characteristics of triaxial behaviour, that is, pressure sensitivity and pressure melting, at least for the strainrate of 10^{-3} s^{-1} . For the lower strainrate of 10^{-5} s^{-1} , Fig. 9 shows widely scattered data and this explains why the corresponding stress-strain curves in Fig. 8 do not fit closely with the data for this strainrate.

The same general conclusions can be drawn with respect to the other two cases of $\sigma : c = 45^\circ$ and 90° , see Figs. 10 and 11. From the shear strength versus confining pressure plots it is observed that pressure sensitivity is most significant when the loading axis is aligned with the c -axis, and least significant when they are at an angle of 90° (only 15% increase in shear strength).

The proposed model assumes that the material is initially isotropic, while most of the sea ice samples that were tested are materially anisotropic. To overcome this problem, verification of the model has been carried out by

assuming that the creep resistance A in different directions is different, and also that the damage parameters, being material dependent constants, also vary with the direction of loading. In other words, if the material were isotropic, A and the damage parameters would be invariant with respect to the direction of loading. For the model $A(0^\circ)/A(45^\circ) = 1.7$, and $A(0^\circ)/A(90^\circ) = 1.2$. It was also found that for sea ice β and γ are much larger than the corresponding values for non-saline ice. The first three rows of Table 2 give the values of these parameters.

The effect of confining pressure on damage parallel to the compressive axis is illustrated in Fig. 12. The suppression of damage due to the confining pressure is very evident. The decomposition of damage into its anisotropic and isotropic components is shown in Fig. 13. In Fig. 13a it is seen that the anisotropic damage due to the maximum principal deviatoric stress is completely suppressed for $\tau > 0.5$, while Fig. 13b shows that the accompanying increase in the distortional stress due to the increase in confining stress actually aggravates damage. However, at $\tau = 0.75$, pressure melting becomes dominant and the distortional stress that can be sustained by the ice reduces significantly, thus resulting in smaller damage, as seen in Fig. 13b. The crossing-over of the curves at small strains in Fig. 13b is attributed to the fact that initially the distortional stress and hence the isotropic damage reduces with increase in confining stress; this is overridden when the enhanced suppression of anisotropic damage by the larger confining stress leads to increase in the distortional stress. Finally, it should be mentioned that since the maximum principal deviatoric stress is always normal to the compressive axis and has no component along this axis, the damage in planes perpendicular to the compressive axis is solely due to the distortional stress and is represented by Fig. 13b.

Jones (1982) performed a series of conventional triaxial tests on freshwater ice at the temperature of -12°C and for strainrates varying between $1.4 \times 10^{-6} \text{ s}^{-1}$ and $1.4 \times 10^{-2} \text{ s}^{-1}$. Fig. 14 reproduces his data and also plots the model predictions using the damage parameters listed in Table 2. The model gives good predictions, particularly for strainrates at and under $1.4 \times 10^{-3} \text{ s}^{-1}$; for the very high strainrates (5.4×10^{-3} and $1.4 \times 10^{-2} \text{ s}^{-1}$), the model slightly overpredicts the shear strength. Note that the shear strength can increase by as much as 100% under confinement for the highest strainrate used in his tests.

To formulate a three-dimensional yield envelope for ice which takes into account pressure sensitivity and pressure melting, Nadreau has recently conducted a series of conventional triaxial tests on saline ice and iceberg ice. Both types of ice are isotropic. The two strainrates used in his tests are 10^{-4} and 10^{-6} s^{-1} . The experimental results for saline ice at the temperatures of 263 K and 268 K, and for iceberg ice at 263 K, are shown in Figs. 15 and 16 respectively. Superimposed on these data are the predictions of the model, which can be seen to capture the overall behaviour very well. For the smaller strainrate, the model predicts little pressure sensitivity. The iceberg ice also displays a greater degree of pressure sensitivity than the saline ice, with approximately 100% and 65% increase in shear strength respectively. The values of A and the damage parameters are shown in Table 2.

5. CONCLUSIONS

The model presented in this paper for describing the continuum damage behaviour of ice under variable loading conditions is based on the generalized Maxwell differential formulation, an anisotropic damage theory and a pressure melting model. Specifically, it is able to (a) describe anisotropic damage

behaviour under multiaxial and non-steady states of stress, (b) capture the pressure sensitivity of ice, and (c) model the pressure melting behaviour of ice. Verification of the model is achieved with several independent sets of data, including those for first-year sea ice and freshwater ice. The following conclusions can be drawn from the work reported in this paper:

1. The damage model is described by 5 parameters, which are used in the damage evolution equations to model the dependence of damage growth rate on the principal stress, the volumetric stress, the effective stress, as well as strainrate and the effect of local damage.

2. The damage model assumes that (a) the damage state can be described by a second rank symmetric tensor, (b) the net stress tensor, which is the locally magnified stress due to area reduction, can be used to specify the damage growth laws, and (c) an averaged net stress tensor is valid for specifying the constitutive laws.

3. Material damage is considered to consist of an isotropic component and an anisotropic component. The former is associated with the J_2 damage law while the latter with the principal stress damage law. Damage due to the distortional stress may be dominant under moderate or large hydrostatic stresses when anisotropic damage is suppressed.

4. The pressure melting model is based on the assumption that the creep resistance parameter A reduces with increase in hydrostatic pressure. This is mathematically achieved through a temperature correction using the phase diagram for ice or a mathematical equation. The relation between A and the corrected temperature is then obtained via the Arrhenius Law for $T < 263$ K or a newly formulated relation for $T > 263$ K.

5. The model can capture well the dominant characteristics of the experimental data by Wang, Mellor, Richter-Menge et al., Jones, Nadreau and

others . In the uniaxial tests, the behaviour of decreasing strength or asymptotically increasing strength with increasing strainrate in the brittle to ductile transition region can be modelled. At strainrates greater than 10^{-2} s^{-1} , the presence of macrocracks precludes a solely continuum description of ice behaviour. Damage is insignificant at small strains and strainrates. Also, strength becomes insensitive to temperature at the brittle end of the strength versus strainrate curve. For the triaxial tests, the effect of microcrack suppression by the volumetric stress can be captured by the model , as verified against the stress-strain curves of Richter-Menge et al. Pressure sensitivity is moderate for sea ice, but is much more significant for freshwater ice. Under large hydrostatic stresses, pressure melting becomes important.

Additional research is needed to resolve several issues; including (a) the experimental verification of the damage tensor, the damage effect tensor, and the net stress tensors for damage evolution and constitutive relations, (b) the development of the model assuming initial material anisotropy as well as initial distribution of pores/damage, (c) a more in-depth exploration of the micromechanics of damage such as the possibility of complete or partial crack closure due to rotation of the stress field with possible effect on damage accumulation, the interaction of microcracks leading to instability , and the influence of the shape of the microdefects (planar/spheroidal/ellipsoidal) on material damage behaviour, (d) the application of the model to stress controlled tests and arbitrary loading histories, and (e) further investigation into the relationship between creep resistance and the hydrostatic stress.

REFERENCES

- Ashby, M.F. and Hallam, S.D. (1986), The Failure of Brittle Solids Containing Small Cracks Under Compressive Stress States, *Acta Metallurgica*, Vol. 34, No. 3, 497-510.
- Chaboche, J.L. (1981), Continuous Damage Mechanics, *Nuclear Engineering and Design* 64, 233-247.
- Chaboche, J.L. (1984), Anisotropic Creep damage in the Framework of Continuum Damage Mechanics, *Nuclear Engineering and Design* 79, 309-319.
- Costin, L.S. (1983), A Microcrack Model for the Deformation and Failure of Brittle Rock, *Journal of Geophysical Research*, Vol. 38, 9485-9492.
- Costin, L.S. (1985a), Time-Dependent Damage and Creep of Brittle Rock, in *Damage Mechanics and Continuum Modelling*, edited by Norris Stubbs and Dusan Krajcinovic, American Society of Civil Engineers, 25-38.
- Costin, L.S. (1985b), Damage Mechanics in the Post-Failure Regime, *Mechanics of Materials* 4, 149-160.
- Dragon, A. and Mroz, Z. (1979), A Continuum Model for Plastic-Brittle Behaviour of Rock and Concrete, *International Journal of Engineering Science*, Vol. 17, 121-137.
- Fonseka, G.U. and Krajcinovic, D. (1981), The Continuous Damage Theory of Brittle Materials, Part 2: Uniaxial and Plane response Modes, *Journal of Applied Mechanics*, Vol. 48, 816-824.
- Hausler, F.U. (1981), Multiaxial Compressive Strength on Saline Ice with Brush-Type Loading Platens, *IAHR 1981, Quebec City, Proceedings*, Vol. 2, 526-539.
- Jones, S.J. (1978), Triaxial Testing of Polycrystalline ice, *Proceedings of the Third International Conference on Permafrost*, Edmonton, Canada, July 1978, 671-674.
- Jones, S.J. (1982), The Confined Compressive Strength of Polycrystalline Ice, *Journal of Glaciology*, Vol. 28, No.98, 171-177.
- Kachanov, M. (1958), On the Time to Failure Under Creep Conditions, *Izv. Akad. Nauk SSSR, Otd. tekhn. n.*, No. 8, 26-31.
- Kachanov, M. (1980), Continuum Modelling of Medium with Cracks, *Journal of the Engineering Mechanics Division, ASCE*, 106, 1039-1051.
- Kachanov, M. (1982), Microcrack Model of Rock Inelasticity, *Mechanics of Materials*, 1, p. 19.
- Kachanov, M. (1985), On a Continuum Modelling of Damage, in *Application of Fracture Mechanics to Cementitious Composites*, NATO-ARW, September 4-7, 1984, Northwestern University, U.S.A., edited by S. P. Shah, 521-531.

- Karr, D.G. (1985), A Damage Mechanics Model for Uniaxial Deformation of Ice, Proceedings, Fourth International Symposium on Offshore Mechanics and Arctic Engineering, Dallas, Texas, February 1985, 227-233.
- Krajcinovic, D. (1983a), Creep of Structures -A Continuous Damage Mechanics Approach, Journal of Structural Mechanics, 11(1), 1-11.
- Krajcinovic, D. (1983b), Constitutive Equations for Damaging Materials, Journal of Applied Mechanics, Vol. 50, 355-360.
- Krajcinovic, D. (1985a), Mechanics of Solids with a Progressively Deteriorating Structure, in Application of Fracture Mechanics to Cementitious Composites, NATO-ARW, September 4-7, 1984, Northwestern University, U.S.A., edited by S. P. Shah, 453-479.
- Krajcinovic, D. (1985b), Constitutive Theories for Solids with Defective Microstructure, in Damage Mechanics and Continuum Modelling, edited by Norris Stubbs and Dusan Krajcinovic, American Society of Civil Engineers, 39-56.
- Krajcinovic, D. (1985c), Continuous Damage Mechanics Revisited: Basic Concepts and Definitions, Journal of Applied Mechanics, Vol. 52, 829-834.
- Krajcinovic, D. and Fonseka, G.U. (1981), The Continuous Damage Theory of Brittle Materials, Part 1: General Theory, Journal of Applied Mechanics, Vol. 48, 809-815.
- Leckie, F.A. and Hayhurst, D.R. (1974), Creep Rupture of Structures, Proc. Royal Soc., London, A340, p. 323.
- Levy, A.J. (1985), A Physically Based Constitutive Equation for Creep-Damaging Solids, Journal of Applied Mechanics, Vol. 52, 615-620.
- Mellor, M. (1983), Mechanical Behaviour of Sea Ice, U.S. Army Cold Regions Research and Engineering Laboratory, CRREL Monograph 83-1, p. 105.
- Murakami, S. (1983), Notion of Continuum Damage Mechanics and its Application to Anisotropic Creep Damage Theory, ASME Journal of Engineering Materials and Technology, Vol. 105, 99-105.
- Murakami, S. and Imaizumi, T. (1982), Mechanical Description of Creep Damage State and its Experimental Verification, Journal de Mecanique Theorique et Appliquee, Vol. 1, 743-761.
- Murakami, S. and Ohno, N. (1978), Inelastic Behaviour of Pressure Vessel and Piping Components, edited by Chang, T.Y. and Krempl, E., PVP-PB-028, ASME, New York, 55-69.
- Murakami, S. and Ohno, N. (1981), A Continuum Theory of Creep and Creep Damage, in Creep in Structures, ed. A.R.S. Ponter, Springer-Verlag, 422-443.
- Murakami, S., Sanomura, Y. and Saitoh, K. (1986), Formulation of

Cross-Hardening in Creep and its Effect on the Creep Damage Process of Copper, ASME Journal of Engineering Materials and Technology, Vol. 108, 167-173.

Nadreau, J.D. (1986), Yield Envelope for Confined Ice, in Ice Technology, edited by T.K.S. Murthy, J.J. Connor and C.A. Brebbia, Proceedings of the First International Conference, Cambridge, Mass. USA, June 1986, Springer-Verlag, 25-36.

Nemat-Nasser, S. and Horri, H. (1982), Compression-Induced Non-Planar Crack Extension with Application to Splitting, Exfoliation, and Rockburst, Journal of Geophysical Research, Vol. 87, No. B8, 6805-6821.

Ortiz, M. (1985), A Constitutive Theory for the Inelastic Behaviour of Concrete, Mechanics of Materials 4, 67-93.

Richter-Menge, J.A., Cox, G.F.N., Perron, N., Durell, G. and Bosworth, H.W. (1985), Triaxial Testing of First-Year Sea Ice, Internal Research Report 877, U.S. Army Cold Regions Research and Engineering Laboratory, Hanover, New Hampshire.

Sinha, N.K. (1984), Intercrystalline Cracking, Grain-Boundary Sliding and Delayed Elasticity at High Temperatures, Journal of Material Science, No. 19, 359-376.

Szyskowski, W. and Glockner, P.G. (1986), On a Multiaxial Constitutive Law for Ice, Mechanics of Materials 5, 49-71.

Ting, S-K and Shyam Sunder, S. (1985), Constitutive Modelling of Sea Ice with Applications to Indentation Problems, Massachusetts Institute of Technology, Center for Scientific Excellence in Offshore Engineering, Departments of Civil Engineering and Ocean Engineering, CSEOE Report No. 3, 15-87.

Ting, S-K and Shyam Sunder, S. (1986), A Rate - Sensitive Model for the Continuum Behaviour of Sea Ice, Cold Regions Science and Technology, Submitted for Publication.

Wu, C.H. (1985), Tension-Compression Test of a Concrete Specimen Via a Structure Damage Theory, in Damage Mechanics and Continuum Modelling, edited by Norris Stubbs and Dusan Krajcinovic, American Society of Civil Engineers, 1-12.

Table 1 : Average Values of A and Damage Parameters (for Zero Salinity and the Temperature of -10°C)

	α	β	γ	c_1	c_2	A
Case 1	67.5	2.5	1	2.4	1.9	185000
Case 2	1.45	0.04	0.0001	0.6	0.1	650000

Table 2 : Specific Values of A and Damage Parameters

	α	β	γ	c_1	c_2	A
Richter-Menge et. al (Columnar Sea Ice)						
$\sigma : c = 0^{\circ}$	1.05	0.41	0.05	0.31	0.1	150000
$\sigma : c = 45^{\circ}$	1.59	0.36	0.07	0.31	0.1	88000
$\sigma : c = 90^{\circ}$	1.10	0.50	0.06	0.31	0.1	127500
Jones (Freshwater Ice)	1.00	0.02	0.0001	0.50	0.1	270000
Nadreau (Saline Ice)	1.45	0.04	0.0001	0.40	0.1	210000
(Iceberg Ice)	1.50	0.04	0.0001	0.40	0.1	260000

FIGURE CAPTIONS

- Figure 1 Representation of Damage and Net Stress by Second Rank Tensors.
- Figure 2 Phase Diagram for Pure Ice.
- Figure 3 Variation of Creep Resistance Parameter A with Temperature.
- Figure 4 Normalized Strength of Columnar Pure and Sea Ice under Constant Strainrate Loading.
- Figure 5 Variation of Normalized Ice Strength Due to Temperature Changes.
- Figure 6 Effect of Strain and Strainrate on Axial Damage.
- Figure 7 Alternative Interpretation of the Variation of Ice Strength with Strainrate.
- Figure 8 Changes in Stress-Strain Response with Increase in Confining Pressure for the Strainrates of 10^{-3} and 10^{-5} s^{-1} ($\sigma : \epsilon = 0^\circ$).
- Figure 9 Normalized Shear Strength Versus Confining Pressure Curves Corresponding to Figure 8.
- Figure 10 Changes in Stress-Strain Response with Increase in Confining Pressure for the Strainrate of 10^{-3} s^{-1} ($\sigma : \epsilon = 45^\circ$ and 90°).
- Figure 11 Normalized Shear Strength Versus Confining Pressure Curves Corresponding to Figure 10.
- Figure 12 Effect of Confining Pressure on Axial Damage.
- Figure 13 Decomposition of Damage into its Anisotropic Component (a) and Isotropic Component (b).
- Figure 14 Shear Strength Versus Confining Pressure Curves for Freshwater Ice at the Temperature of -12°C .
- Figure 15 Shear Strength Versus Confining Pressure Curves for Saline Ice at the Temperatures of -10°C and -5°C .
- Figure 16 Shear Strength Versus Confining Pressure Curves for Iceberg Ice at the Temperature of -10°C .

